LETTER

MFN1 structures reveal nucleotide–triggered dimerization critical for mitochondrial fusion

Yu–Lu Cao[1], Shuxia Meng[2], Yang Chen[1], Jian–Xiong Feng[1], Dong–Dong Gu[1], Bing Yu[1], Yu–Jie Li[1], Jin–Yu Yang[1], Shuang Liao[1], David C. Chan[2] & Song Gao[1]

Mitochondria are double-membraned organelles with variable shapes influenced by metabolic conditions, developmental stage, and environmental stimuli[1–4]. Their dynamic morphology is a result of regulated and balanced fusion and fission processes[5,6]. Fusion is crucial for the health and physiological functions of mitochondria, including complementation of damaged mitochondrial DNAs and the maintenance of membrane potential[6–8]. Mitofusins are dynamin-related GTPases that are essential for mitochondrial fusion[9,10]. They are embedded in the mitochondrial outer membrane and thought to fuse adjacent mitochondria via combined oligomerization and GTP hydrolysis[11–13]. However, the molecular mechanisms of this process remain unknown. Here we present crystal structures of engineered human MFN1 containing the GTPase domain and a helical domain during different stages of GTP hydrolysis. The helical domain is composed of elements from widely dispersed sequence regions of MFN1 and resembles the 'neck' of the bacterial dynamin-like protein. The structures reveal unique features of its catalytic machinery and explain how GTP binding induces conformational changes to promote GTPase domain dimerization in the transition state. Disruption of GTPase domain dimerization abolishes the fusogenic activity of MFN1. Moreover, a conserved aspartate residue trigger was found to affect mitochondrial elongation in MFN1, probably through a GTP-loading-dependent domain rearrangement. Thus, we propose a mechanistic model for MFN1-mediated mitochondrial tethering, and our results shed light on the molecular basis of mitochondrial fusion and mitofusin-related human neuromuscular disorders[14].

We constructed an internally modified human MFN1 (MFN1$_{IM}$) composed of the GTPase (G) domain (residues 75–336) and a four-helix-bundle that we term helical domain 1 (HD1; Fig. 1a, b, Extended Data Fig. 1a–g and Extended Data Table 1). The G domain contains a central eight-stranded β-sheet surrounded by eight α-helices. Compared to the canonical GTPase Ras, the G domain of MFN1 has two extra lobes that shield the nucleotide-binding pocket, and a specific short α-helix (α2'^{G}) sitting between α4^G and β6^G (Fig. 1c). Lobe 1, containing two β-strands (β1'^{G} and β2'^{G}) and an α-helix (α1'^{G}), is located between β2^G and β3^G, whereas lobe 2, consisting of an α-helix (α3'^{G}) and a loop, is located between β6^G and α5^G (Extended Data Fig. 2a). The four α-helices of HD1, derived from widely dispersed sequence regions, form a vast and conserved hydrophobic network (Fig. 1a, d and Extended Data Fig. 2b). HD1 is connected to the G domain via Arg74 at the C-terminal end of α2^H and Lys336 between α5^G and α3^H (Fig. 1b). The N terminus of α1^H substantially contacts the G domain (Extended Data Fig. 2c–e). On the other side of HD1, part of the artificial linker folds into an α-helix extending α3^H (Fig. 1b). This is in agreement with the secondary structure prediction for the replaced residues (Extended Data Fig. 3), suggesting that α3^H may be longer in full-length MFN1.

The overall topology of MFN1$_{IM}$ is typical of the dynamin superfamily[15–20] (Extended Data Fig. 4). Apart from the G domain, the MFN1$_{IM}$ HD1 is particularly consistent with the neck of the *Nostoc punctiforme* bacterial dynamin-like protein (BDLP), which was suggested to mediate membrane fusion in bacteria[21] (Extended Data Figs 2a, 4, 5a). Given the compact organization of HD1 and the predicted secondary structure (Extended Data Fig. 3), the missing portion of MFN1 (excluding the transmembrane domain) from MFN1$_{IM}$ is likely to fold into a helix-rich domain resembling the 'trunk' and 'paddle' of BDLP[21]. We term this putative region helical domain 2 (HD2).
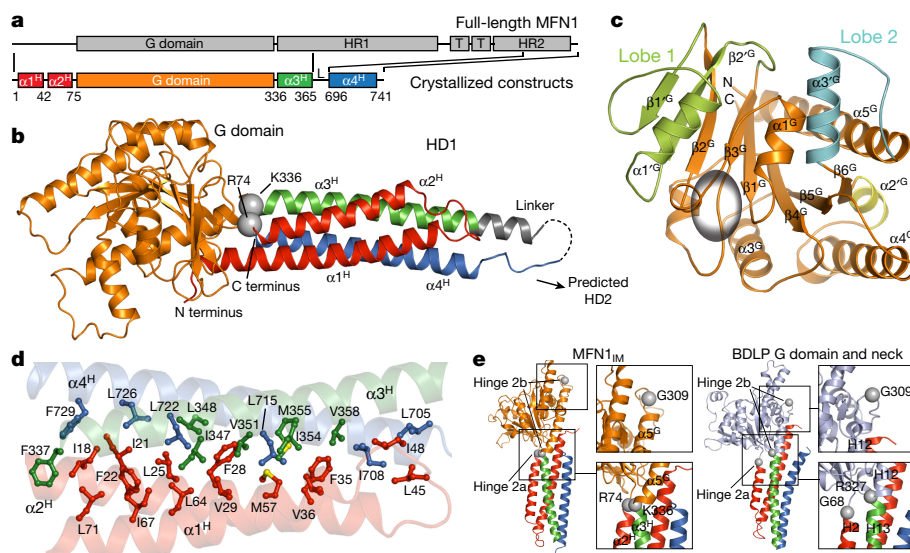

Figure 1 | Overall structure of MFN1$_{IM}$.
a, Schematic representation showing the organization of MFN1$_{IM}$ based on full-length MFN1 with the conventional terminology. G domain, GTPase domain; HR1, heptad repeat region 1; T, transmembrane region. Elements for MFN1$_{IM}$ are assigned according to the structure. L denotes the artificial linker. Borders of each element are indicated by residue numbers. **b**, Structure of MFN1$_{IM}$. α-helices of HD1 are differentially coloured to specify their distribution on the primary structure as in **a**. The artificial linker is in grey. Disordered loop is shown as dashed lines. The Cα atoms of Arg74 and Lys336 that link the G domain and HD1 are shown as grey spheres. **c**, The G domain of MFN1$_{IM}$. Lobes 1, 2 and α2'^{G} are colour-specified. The core region corresponding to Ras is in orange and the GTPase active site is indicated by an ellipsoid. **d**, Hydrophobic network within HD1. Side chains of the residues involved in the network are shown in the same colour as the helices they belong to. **e**, Comparison between the putative hinge 2 of MFN1$_{IM}$ and BDLP.

[1]State Key Laboratory of Oncology in South China, Collaborative Innovation Center for Cancer Medicine, Sun Yat-sen University Cancer Center, Guangzhou 510060, China. [2]Division of Biology and Biological Engineering, California Institute of Technology, Pasadena, California 91125, USA.
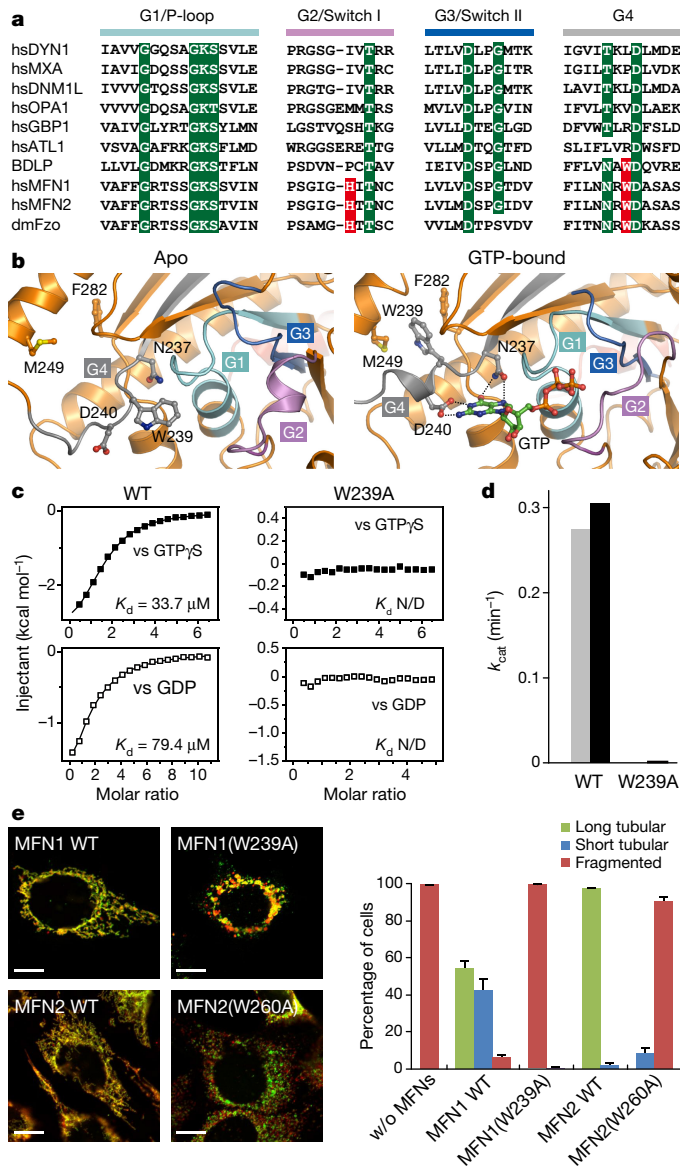
Figure 2 | A tryptophan switch mediates nucleotide binding. a, Sequence alignment of the G1–G4 elements for different dynamin superfamily members. Conventional motifs/residues are highlighted in green. Key residues responsible for nucleotide binding and catalysis of MFN1 are highlighted in red. dm, *Drosophila melanogaster*; hs, *Homo sapiens*. **b,** Structural details of the nucleotide-binding pocket in nucleotide-free (or apo, left) and GTP-bound (right) states. G1–G4 are coloured as in **a**. **c,** Binding affinities (dissociation constant, K_d) to GTPγS and GDP for wild-type MFN1$_{IM}$ and MFN1$_{IM}$(W239A) were measured by isothermal titration calorimetry (ITC). N/D, not determined. **d,** GTP turnover rates of wild-type MFN1$_{IM}$ and MFN1$_{IM}$(W239A). Results from two separated experiments are individually presented in grey and black for each protein. **e,** Mitochondrial elongation assay for wild-type (WT) and the tryptophan switch mutants of MFN1 and MFN2, when expressed in *Mfn1/Mfn2*-null cells. In the representative images, red and green fluorescence indicate mitochondria and Myc-tagged protein, respectively, for the MFN1 experiment, and vice versa for the MFN2 experiment. The data are quantified on the right. w/o MFNs: without MFN1 and MFN2. For each construct, 100 cells were scored in biological triplicate. Error bars indicate s.e.m. Scale bars, 10 μm.

When bound to tubulated liposomes in the presence of GMPPNP, BDLP bears G domain–neck and neck–trunk rearrangements via so-called hinge 2 and hinge 1 (ref. 22). Notably, Lys336 of MFN1$_{IM}$ exactly overlaps with BDLP Arg327 at hinge 2b, whereas MFN1$_{IM}$ Gly309 and Arg74 also have counterparts in BDLP (Gly309 in hinge 2b

and Gly68 in hinge 2a) at equivalent positions (Fig. 1e). Mutation of these hinge-2-related residues diminished GTPase activity and mitochondrial elongation, although the G domain and HD1 exhibited only limited relative movement in different nucleotide-loading states (Extended Data Fig. 5b–e). Similar to dynamins, the potential hinge 1 between HD1 and predicted HD2 (368-YSVEER-373 and 692-EEEIAR-697) lacks overall conservation among mitofusins (Extended Data Fig. 3). A proline insertion in 692-EEEIAR-697 abolished mitochondrial elongation activity (Extended Data Fig. 5e, f). Altogether, full-length MFN1 may undergo conformational changes similar to BDLP when mediating outer mitochondrial membrane (OMM) fusion via aforementioned hinges.

G1–G4 elements of GTPases are essential for binding and hydrolysis of GTP (Fig. 2a). Notably, in the nucleotide-free (apo) MFN1$_{IM}$ structure, the nucleotide-binding pocket is occupied by the bulky side chain of Trp239 from G4, a residue conserved only in mitofusins and BDLP (Fig. 2b). Loading of GTP drives Trp239 away, causing it to wedge into a wide hydrophobic groove formed by Met249 from α4^G and Phe282 from β6^G. This rearrangement allows the suitable positioning of Asn237 and Asp240 to dock the guanine base (Fig. 2b). Mutation of Trp239 to alanine abolished nucleotide-binding and GTPase activity of MFN1$_{IM}$ (Fig. 2c, d). Both MFN1(W239A) and the corresponding MFN2 mutant MFN2(W260A) were nonfunctional for mitochondrial elongation (Fig. 2e), manifesting the importance of this tryptophan switch. When accommodating a nucleotide, MFN1$_{IM}$ uses α2'^{G} to loosely buttress the guanine from a vertical orientation, and a large area of the nucleotide is thus exposed. This feature is shared by BDLP but not with dynamin-1 (refs 21,23), in which the nucleotide is tightly wrapped (Extended Data Fig. 5g).

Whereas the apo and GTP structures are monomeric, MFN1$_{IM}$ forms a homodimer in the presence of the transition state mimic GDP•AlF$_4^-$ (Extended Data Fig. 6a). Dimerization is mediated by association of the G domains across the nucleotide-binding pocket, and the HD1s protrude in opposite directions from the dimer axis (Fig. 3a). Major interactions of this 995 Å^2 'G interface' include a pair of symmetrical, parallel aligned salt bridges between Arg238 in the G4 element and Glu209 in the loop between β3^G and α3^G (Fig. 3b). Flanking this central salt-bridge pair, close in *trans* contacts are also observed between Lys99–Glu245, His144–Glu247, and His147–Asp251. In addition, the side chain of Tyr248 inserts into the groove between switch I and α1'^{G} of the other molecule (Fig. 3b). G domain dimerization has been found in several dynamin superfamily members in the transition state of GTP hydrolysis[23–25]. Compared to the approximately 2,500 Å^2 G interface of dynamin-1 (ref. 23) involving extensive hydrogen bonds and hydrophobic associations, the substantially smaller G interface of MFN1$_{IM}$ is dictated by charged interactions, and no in *trans* stabilization of the nucleotides is observed (Fig. 3c).

To verify the functional relevance of G-domain-mediated dimerization, we performed mutagenesis studies on residues Glu209 and Arg238. Whereas GDP•AlF$_4^-$ induced the formation of MFN1$_{IM}$ dimers in analytical gel filtration coupled to right angle light scattering (RALS) assays, MFN1$_{IM}$(E209A) and MFN1$_{IM}$(R238A) failed to dimerize (Fig. 3d). Moreover, the two mutants lacked stimulated protein-concentration-dependent GTPase activity (Fig. 3e), even though they bound guanine nucleotides with wild-type affinity (Fig. 3f). These results suggest that GTPase activation is mediated by dimerization via the G interface. In addition, MFN1$_{IM}$(E209A) and MFN1$_{IM}$(R238A) showed suppressed liposome tethering activity *in vitro* (Extended Data Fig. 6b). Both MFN1(E209A) and MFN1(R238A), as well as the corresponding MFN2 mutants MFN2(E230A) and MFN2(R259A), failed to elongate mitochondria (Fig. 3g). Thus, G domain association of mitofusins during the transition state of GTP hydrolysis is an indispensable step for OMM fusion. In addition, mutations of most other residues involved in the G interface also impinge dimerization, GTP hydrolysis and mitochondrial elongation to various extents (Extended Data Fig. 6c–e).
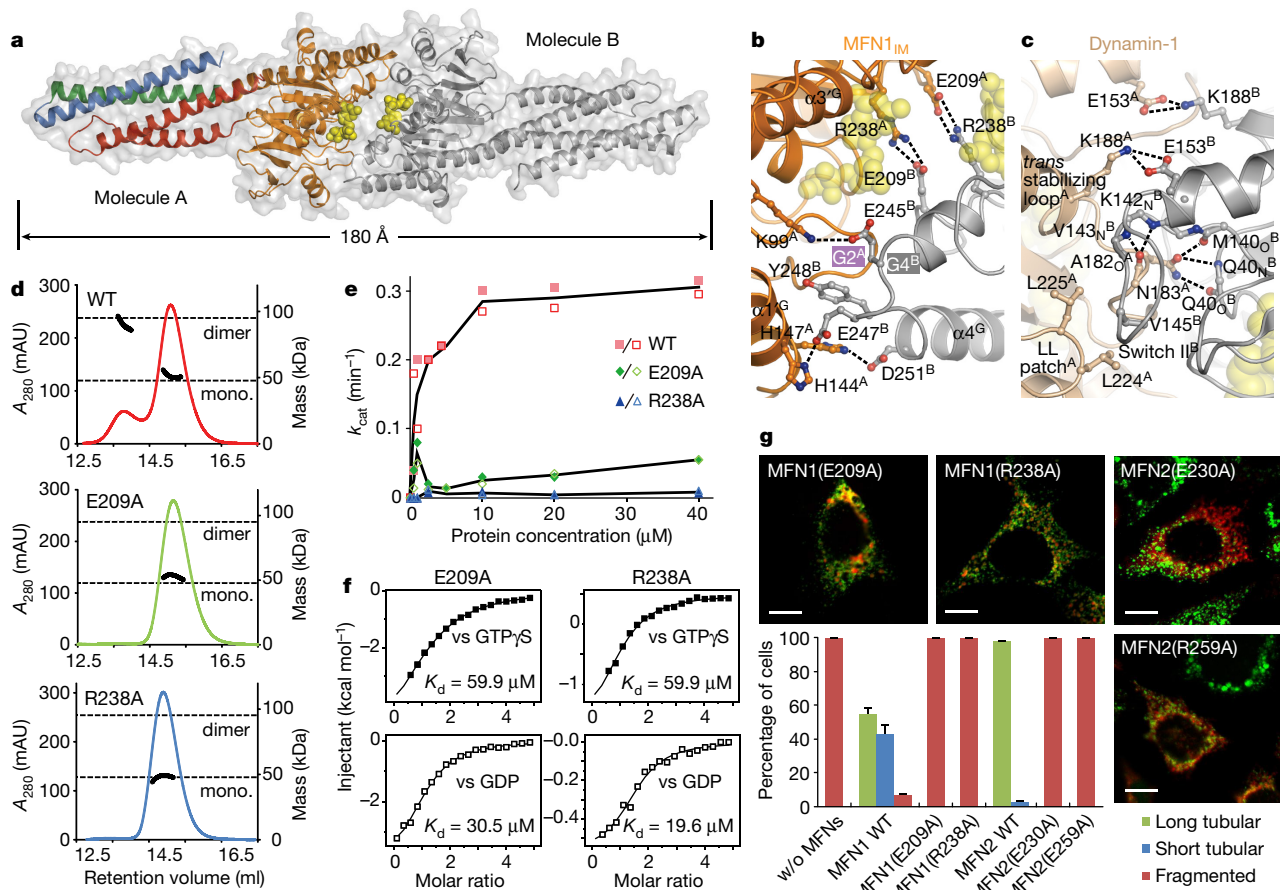
Figure 3 | Dimerization of MFN1$_{IM}$ via the G domain. a, The MFN1$_{IM}$ dimer in the transition-like state, with transparent surface representation. Molecule A is coloured as in Fig. 1b, molecule B is in grey. GDP is shown as yellow spheres. **b**, Details of the G interface of MFN1$_{IM}$. Only one side of the G interface is shown for other involved residues. **c**, Details of the G interface of human dynamin-1 in the transition state (PDB code 2X2E). Region corresponding to **b** is shown. **d**, Dimerization properties of wild-type MFN1$_{IM}$ and E209A and R238A mutants in the presence of GDP•AlF$_4^-$ were assayed in analytical gel filtration coupled to RALS. Calculated molecular masses at the absorption peak of 280 nm are plotted in black. mAU, milli-absorption units. **e**, GTP turnover rates of wild-type MFN1$_{IM}$, and E209A and R238A mutants were measured at 7 different protein concentrations. For each group, the average k_{cat} values from two separate experiments at each protein concentration are traced by line charts. **f**, Binding affinities to GTPγS and GDP for MFN1$_{IM}$ mutants E209A and R238A. **g**, Mitochondrial elongation assay with quantification for MFN1(E209A) and MFN1(R238A), and related mutants MFN2(E230A) and MFN2(R259A). For each construct, 100 cells were scored in biological triplicate; representative images are shown. Error bars indicate s.e.m. Scale bars, 10 μm.

Nucleotide binding induces conformational changes in the residues defining the G dimer interface. In the nucleotide-free state, the conformation of MFN1$_{IM}$ disfavours dimerization: Arg238 is blocked by the carbonyl oxygens of Ala241 and Ala243, whereas Glu209 and Glu245 are attracted by Arg253 (Extended Data Fig. 6f). GTP-loading-induced rearrangement of the G4 element translocates Trp239 to push Arg253 aside towards Glu316. As a result, Glu209, Glu245 and Arg238 are released and become solvent-facing, allowing for G domain dimerization.

During GTP hydrolysis, the conformationally flexible switch regions must be stabilized to favour catalysis. In our MFN1$_{IM}$ structure solved from co-crystallization with GDP•AlF$_4^-$, although the AlF$_4^-$ moiety is absent, the switch I holds a catalysis-compatible conformation analogous to those of other dynamin superfamily members in the transition state (Fig. 4a and Extended Data Fig. 7a–d). Notably, unlike many dynamin-related proteins, switch I of nucleotide-free MFN1$_{IM}$ is fixed in a conformation distinct from that in the transition-like state by a hydrophobic network involving G2 element and α1'^{G}, indicating that switch I is rearranged through dimerization of the G domains (Figs 2b, 3b and Extended Data Fig. 7a).

Efficient GTP hydrolysis requires the neutralization of the negative charge developing between the β- and γ-phosphates in the transition state. A sodium ion coordinated by a QS motif in the P-loop takes over this role in dynamin-1 (ref. 23), whereas atlastin-1 possesses a *cis*-arginine finger in the P-loop[24] (Fig. 4a). However, these motifs are not present in MFN1. Instead, a mitofusin-specific His107 in switch I stretches to the β-phosphate of GDP with a similar position as the charge-compensating ion/residue of dynamin-1 and atlastin-1. Furthermore, the side chain of His107 is coordinated by the carbonyl oxygen of Gly104, which corresponds to Gly60 of dynamin-1 and Gly114 of atlastin-1 (Figs 2a, 4a). Mutation of His107 to alanine did not perturb the binding of guanine nucleotides but eliminated the GTPase activity of MFN1$_{IM}$ (Fig. 4b, c). *Mfn1/2*-null mouse embryonic fibroblasts (MEFs) transfected with either MFN1(H107A) or the corresponding mutant MFN2(H128A) were defective in mitochondrial elongation (Fig. 4d). Thus, we propose this His107 finger as a charge-compensating factor during catalysis. The catalytic water responsible for the nucleophilic attack on the γ-phosphate was not observable, probably owing to the absence of the AlF$_4^-$ moiety.

Compared to other scission-related dynamin family members, MFN1$_{IM}$ shows extraordinarily weak GTPase activity (Fig. 2d). The stable conformation of switch I and the shielded GTP-binding pocket in the nucleotide-free state may account for this feature (Fig. 4e). Slow GTP turnover, exemplified by BDLP[22] and EHD2 (ref. 15), has been suggested to favour self-assembly over disassembly, and thus promote membrane fusion[26].
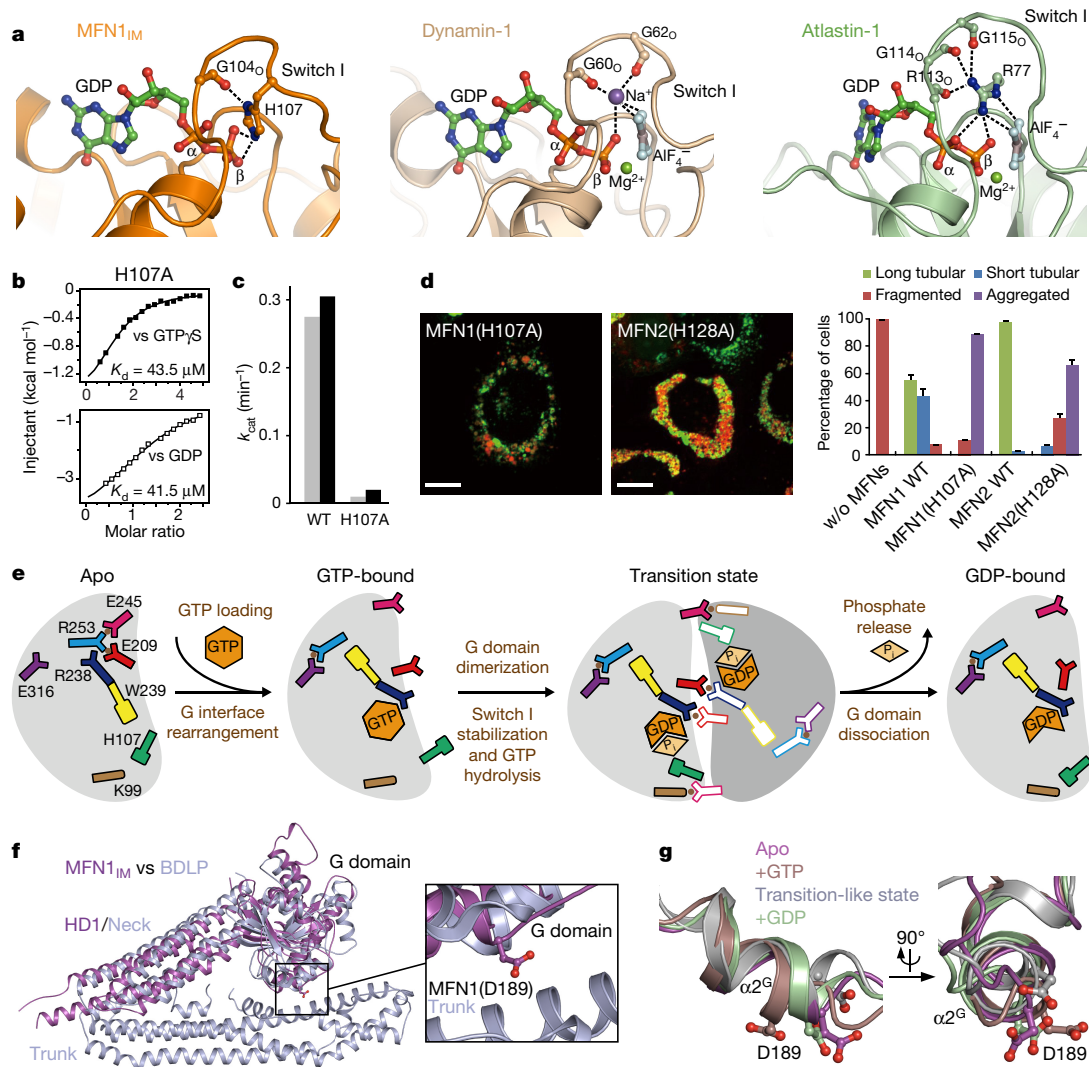
Figure 4 | Catalytic machinery of MFN1. a, Comparison of the catalytic centres of MFN1 (transition-like state), dynamin-1 (PDB code 2X2E) and atlastin-1 (PDB code 4IDO). **b**, Binding affinities of MFN1$_{IM}$(H107A) to GTPγS and GDP. **c**, GTP turnover rates of wild-type MFN1$_{IM}$ and MFN1$_{IM}$(H107A). Results from two separated experiments are presented for each protein. **d**, Mitochondrial elongation assay with quantification for MFN1(H107A) and related mutant MFN2(H128A). For each construct, 100 cells were scored in biological triplicate; representative images are shown. Error bars indicate s.e.m. Scale bars, 10 μm. **e**, Schematic drawing

summarizing the rearrangements in the G domain during GTP hydrolysis. G domains are coloured grey. Residues and nucleotides are colour/shape-specified. Salt bridges are specified by brown dots between involved residues. P_i denotes phosphate ion. **f**, Superposition of nucleotide-free MFN1$_{IM}$B construct and BDLP (PDB code 2J69) with the predicted-HD2-facing Asp189 of MFN1 specified. **g**, Structural comparison of MFN1$_{IM}$ in different nucleotide-loading states at α2^G reveals distinct orientation of Asp189 in the GTP-bound state from other states.

We also purified a near-full-length construct termed MFN1$_{\Delta TM}$ that contains the G domain, HD1 and HD2, but lacks the transmembrane domain (Extended Data Fig. 8a, b). MFN1$_{\Delta TM}$ elutes as a stable dimer in RALS assays without nucleotide (Extended Data Fig. 8c). This dimer, possibly mediated by HD2, may relate to the 180-kDa stable complex of rat MFN1 found in sedimentation studies[27]. Moreover, MFN1$_{\Delta TM}$ oligomerizes only when GDP•AlF$_4^-$ is present (Extended Data Fig. 8d), consistent with the previous observation that the 180-kDa MFN1 complex can form higher-order oligomers when incubated with GTP but not with GTPγS[27]. MFN1$_{\Delta TM}$ with either Glu209Ala or Arg238Ala mutations failed to oligomerize (Extended Data Fig. 8e), indicating that oligomerization is dependent on the G interface.

In the apo and GMPPNP-bound states, the neck and trunk of BDLP take either a 'closed' or 'open' conformation[21,22], and the contact between the G domain and the trunk may stabilize the former. Given the structural congruence with BDLP, MFN1 may also adopt this feature. A conserved Asp189 potentially participates in the plausible G-domain–HD2 contact (Fig. 4f). This surface residue located on α2^G

is differently oriented between nucleotide-free and GTP-bound states, and in latter case its side chain swings away from the HD2 (Fig. 4g, Extended Data Fig. 8f, g). MFN1(D189A) led to mitochondrial clumping (Extended Data Fig. 8h).

Our data highlight the role of G domain dimerization, regulated by guanine nucleotide, in membrane fusion mediated by mitofusin. GTP loading may induce a conformational change from the closed tethering-constrained state to the open tethering-permissive state, possibly involving the Asp189 trigger. In the open state, stretched MFN1 molecules allow efficient tethering of two OMMs with a distance of as far as 30 nm. During GTP hydrolysis, HD2 may fold back to the closed state to bring opposing membranes in close proximity (Extended Data Fig. 9a–c). An analogous model based on the BDLP1 structure has been proposed[28]. This process may be reversible and controllable by local GTP concentration and MFN1 density, so that excessive tethering can be avoided.

A key issue to be resolved is the reconciliation of this model with the previous MFN1 tethering model, in which an antiparallel coiled coil

at the C terminus had a central role[13,29]. One possibility is that MFN1 operates through sequential tethering events, an initial one using nucleotide-regulated, G domain dimerization followed by closer apposition via the coiled coil. For this sequence to happen, a large energy barrier must be overcome to detach $\alpha 4^H$ from the large hydrophobic network in HD1. It should also be noted that the G domain association of MFN1 may also occur in *cis*, as both forms have been proposed to have functions in BDLP[22] and atlastin-1 (ref. 30).

Online Content Methods, along with any additional Extended Data display items and Source Data, are available in the online version of the paper; references unique to these sections appear only in the online paper.

1. Shaw, J. M. & Nunnari, J. Mitochondrial dynamics and division in budding yeast. *Trends Cell Biol.* **12,** 178–184 (2002).
2. Karbowski, M. & Youle, R. J. Dynamics of mitochondrial morphology in healthy cells and during apoptosis. *Cell Death Differ.* **10,** 870–880 (2003).
3. Youle, R. J. & van der Bliek, A. M. Mitochondrial fission, fusion, and stress. *Science* **337,** 1062–1065 (2012).
4. Mishra, P. & Chan, D. C. Metabolic regulation of mitochondrial dynamics. *J. Cell Biol.* **212,** 379–387 (2016).
5. Yaffe, M. P. The machinery of mitochondrial inheritance and behavior. *Science* **283,** 1493–1497 (1999).
6. Chan, D. C. Fusion and fission: interlinked processes critical for mitochondrial health. *Annu. Rev. Genet.* **46,** 265–287 (2012).
7. Nakada, K. *et al.* Inter-mitochondrial complementation: Mitochondria-specific system preventing mice from expression of disease phenotypes by mutant mtDNA. *Nat. Med.* **7,** 934–940 (2001).
8. Friedman, J. R. & Nunnari, J. Mitochondrial form and function. *Nature* **505,** 335–343 (2014).
9. Santel, A. & Fuller, M. T. Control of mitochondrial morphology by a human mitofusin. *J. Cell Sci.* **114,** 867–874 (2001).
10. Praefcke, G. J. & McMahon, H. T. The dynamin superfamily: universal membrane tubulation and fission molecules? *Nat. Rev. Mol. Cell Biol.* **5,** 133–147 (2004).
11. Rojo, M., Legros, F., Chateau, D. & Lombès, A. Membrane topology and mitochondrial targeting of mitofusins, ubiquitous mammalian homologs of the transmembrane GTPase Fzo. *J. Cell Sci.* **115,** 1663–1674 (2002).
12. Chen, H. *et al.* Mitofusins Mfn1 and Mfn2 coordinately regulate mitochondrial fusion and are essential for embryonic development. *J. Cell Biol.* **160,** 189–200 (2003).
13. Koshiba, T. *et al.* Structural basis of mitochondrial tethering by mitofusin complexes. *Science* **305,** 858–862 (2004).
14. Ranieri, M. *et al.* Mitochondrial fusion proteins and human diseases. *Neurol. Res. Int.* **2013,** 293893 (2013).
15. Daumke, O. *et al.* Architectural and mechanistic insights into an EHD ATPase involved in membrane remodelling. *Nature* **449,** 923–927 (2007).
16. Gao, S. *et al.* Structure of myxovirus resistance protein a reveals intra- and intermolecular domain interactions required for the antiviral function. *Immunity* **35,** 514–525 (2011).
17. Faelber, K. *et al.* Crystal structure of nucleotide-free dynamin. *Nature* **477,** 556–560 (2011).
18. Ford, M. G., Jenni, S. & Nunnari, J. The crystal structure of dynamin. *Nature* **477,** 561–566 (2011).
19. Byrnes, L. J. & Sondermann, H. Structural basis for the nucleotide-dependent dimerization of the large G protein atlastin-1/SPG3A. *Proc. Natl Acad. Sci. USA* **108,** 2216–2221 (2011).
20. Bian, X. *et al.* Structures of the atlastin GTPase provide insight into homotypic fusion of endoplasmic reticulum membranes. *Proc. Natl Acad. Sci. USA* **108,** 3976–3981 (2011).
21. Low, H. H. & Löwe, J. A bacterial dynamin-like protein. *Nature* **444,** 766–769 (2006).
22. Low, H. H., Sachse, C., Amos, L. A. & Löwe, J. Structure of a bacterial dynamin-like protein lipid tube provides a mechanism for assembly and membrane curving. *Cell* **139,** 1342–1352 (2009).
23. Chappie, J. S., Acharya, S., Leonard, M., Schmid, S. L. & Dyda, F. G domain dimerization controls dynamin's assembly-stimulated GTPase activity. *Nature* **465,** 435–440 (2010).
24. Byrnes, L. J. *et al.* Structural basis for conformational switching and GTP loading of the large G protein atlastin. *EMBO J.* **32,** 369–384 (2013).
25. Rennie, M. L., McKelvie, S. A., Bulloch, E. M. & Kingston, R. L. Transient dimerization of human MxA promotes GTP hydrolysis, resulting in a mechanical power stroke. *Structure* **22,** 1433–1445 (2014).
26. Hoppins, S. & Nunnari, J. The molecular mechanism of mitochondrial fusion. *Biochim. Biophys. Acta* **1793,** 20–26 (2009).
27. Ishihara, N., Eura, Y. & Mihara, K. Mitofusin 1 and 2 play distinct roles in mitochondrial fusion reactions via GTPase activity. *J. Cell Sci.* **117,** 6535–6546 (2004).
28. Knott, A. B., Perkins, G., Schwarzenbacher, R. & Bossy-Wetzel, E. Mitochondrial fragmentation in neurodegeneration. *Nat. Rev. Neurosci.* **9,** 505–518 (2008).
29. Franco, A. *et al.* Correcting mitochondrial fusion by manipulating mitofusin conformations. *Nature* **540,** 74–79 (2016).
30. Liu, T. Y. *et al.* Cis and trans interactions between atlastin molecules during membrane fusion. *Proc. Natl Acad. Sci. USA* **112,** E1851–E1860 (2015).

Author Contributions S.G. and D.C.C. conceived the project. Y.-L.C. made the constructs, purified proteins, and performed crystallographic and biochemical experiments. S.M. carried out mitochondrial elongation assays. Y.C. performed ITC measurements and helped with collection of X-ray diffraction data. J.-X.F., B.Y. and Y.-J.L. performed cloning and purification for some of the MFN1$_{IM}$ mutants. D.-D.G. performed some of the SEC-RALS experiments, D.-D.G., J.-Y.Y. and S.L. helped with crystallization experiments. Y.-L.C., S.L. and S.G. solved the structures. Y.-L.C., D.C.C. and S.G. wrote the paper.

Author Information Reprints and permissions information is available at www.nature.com/reprints. The authors declare no competing financial interests. Readers are welcome to comment on the online version of the paper. Correspondence and requests for materials should be addressed to S.G. (gaosong@sysucc.org.cn).

Reviewer Information *Nature* thanks M. Ford and the other anonymous reviewer(s) for their contribution to the peer review of this work.

METHODS

No statistical methods were used to predetermine sample size. The experiments were not randomized, and investigators were not blinded to allocation during experiments and outcome assessment.

Protein expression and purification. cDNAs of all truncated human MFN1 constructs, including those for crystallization and indicated mutants for biochemical assays were individually cloned into a modified pET28 vector. For constructs used in co-crystallization with GTP, an extra Thr109Ala mutation was introduced to the MFN1$_{IM}$C construct to suppress the GTPase activity. Details of these constructs are illustrated in Extended Data Fig. 1a. For MFN1$_{\Delta TM}$, residues 580–631 were replaced by an (SAA)$_5$ linker. For MFN1$_{IM}$ and corresponding mutants, recombinant proteins containing an N-terminal His$_6$-tag followed by a cleavage site for PreScission protease (PSP) were expressed in *Escherichia coli Rosetta* (DE3) cells. Transformed bacteria were cultured at 37 °C before induced with 0.1 mM isopropyl-1-thio-β-D-galactopyranoside (IPTG) at an OD$_{600\,nm}$ of 0.6, and grown overnight at approximately 17–18 °C. Cells expressing MFN1$_{IM}$ were lysed in 50 mM HEPES, pH 7.5, 400 mM NaCl, 5 mM MgCl$_2$, 30 mM imidazole, 1 μM DNase I, 1 mM phenylmethanesulfonylfluoride (PMSF) and 2.5 mM β-mercaptoethanol (β-ME) using a cell disruptor (JNBIO) and subjected to centrifugation at 40,000g for 1 h. The supernatant was filtered and applied to a Ni-NTA (first Ni-NTA) column (GE Healthcare) equilibrated with binding buffer 1 containing 20 mM HEPES, pH 7.5, 400 mM NaCl, 5 mM MgCl$_2$, 30 mM imidazole and 2.5 mM β-ME. After washed with binding buffer 1, proteins were eluted with elution buffer containing 20 mM HEPES, pH 7.5, 400 mM NaCl, 5 mM MgCl$_2$, 300 mM imidazole and 2.5 mM β-ME. Eluted proteins were incubated with 20 μg glutathione S-transferase (GST)-fused PSP to remove the His$_6$-tag and dialysed overnight against binding buffer 2 containing 20 mM HEPES, pH 7.5, 400 mM NaCl, 5 mM MgCl$_2$ and 2.5 mM β-ME. After dialysis, PSP was removed using a GST column. The protein was re-applied to a second Ni-NTA column equilibrated with binding buffer 2. Binding buffer 1 was used to elute the proteins which were subsequently loaded onto a Superdex200 16/60 column (GE Healthcare) equilibrated with gel filtration buffer containing 20 mM HEPES, pH 7.5, 150 mM NaCl, 5 mM MgCl$_2$ and 1 mM dithiothreitol (DTT). The proteins eluted in a discrete peak corresponding to a molecular mass of approximately 50 kDa. Cell lysis and protein purification were both performed at 4 °C. The selenomethionine (SeMet) derivative of MFN1$_{IM}$B was expressed in *E. coli Rosetta* (DE3) in M9 minimal media. For 1 l bacteria culture, 100 mg lysine, 100 mg phenylalanine, 100 mg threonine, 50 mg isoleucine, 50 mg leucine, 50 mg valine and 60 mg SeMet were added when OD$_{600\,nm}$ reached 0.5. The cells were then induced with 100 μM IPTG and cultured at 18 °C for 24 h. Purification protocols for the SeMet derivative were the same as those of native protein. Mutants used in RALS, ITC and GTP hydrolysis assays were all based on MFN1$_{IM}$C, unless specified. Structure of MFN1$_{IM}$B in the nucleotide-free state (assigned PDB code 5GO4) was used in Fig. 1 are representative.

Constructs based on MFN1$_{\Delta TM}$ each possess an extra Strep-tag that was inserted between the His$_6$-tag and PSP cleavage site. Cells expressing MFN1$_{\Delta TM}$ (wild type or mutants) were collected and lysed in 50 mM HEPES, pH 7.5, 400 mM NaCl, 5 mM MgCl$_2$, 30 mM imidazole, 1% Tween-20, 1 μM DNase I, 1 mM PMSF and 2.5 mM β-ME with a cell disruptor (JNBIO). After centrifugation at 40,000g for 1 h, the supernatant was filtered and applied to a Ni-NTA column with binding buffer 3 containing 20 mM HEPES, pH 7.5, 400 mM NaCl, 5 mM MgCl$_2$, 30 mM imidazole, 1% Tween-20 and 2.5 mM β-ME. Proteins were eluted with elution buffer after washed with binding buffer 1 and reapplied to a StrepTactin column (GE Healthcare) equilibrated with binding buffer 2. Binding buffer 2 containing extra 2.5 mM desthiobiotin was used to elute the proteins. After the tags and PSP were removed in the same way as for MFN1$_{IM}$, proteins were applied to gel filtration using a Superdex200 16/60 column equilibrated with gel filtration buffer for GTPase assays or buffer containing 20 mM HEPES, pH 7.2, 30 mM NaCl, 5 mM MgCl$_2$ and 1 mM DTT for RALS assays.

Protein crystallization. Purified MFN1$_{IM}$ constructs were pre-incubated with corresponding nucleotides to tenfold concentration relative to protein for 2 h before being crystallized at 20 °C via hanging drop vapour diffusion by mixing equal volumes of protein (approximately 15–30 mg ml^{-1}) and reservoir solution. Crystals of native and SeMet MFN1$_{IM}$B (apo) grew from 0.2 M sodium citrate tribasic dehydrate and 20–22% PEG 3350 overnight in the presence of GMPPCP. These crystals were then soaked in reservoir solution mixed with an equal volume of gel filtration buffer supplemented with 18–20% PEG 400 for cryo-protection. GTP bound MFN1$_{IM}$C(T109A) grew in 1 mM ZnCl$_2$, 100 mM Tris-HCl, pH 8.0–9.0, 15–16% PEG 3350, 10–15% glycerol overnight and cryo-protected by reservoir solution containing extra 15% ethylene glycol. Crystals of MFN1$_{IM}$C in transition state were obtained in 100 mM MES, pH 6.0, 240 mM NaCl, 36% pentaerythriol propoxylate (5/4 PO/OH) in the presence of tenfold GDP, tenfold AlCl$_3$ and 100-fold NaF, and directly flash-frozen in liquid nitrogen. Crystals of GDP-bound MFN1$_{IM}$C(T109A)

grew in 0.2 M ammonium citrate tribasic and 20% PEG 3350 for 5 days in the present of tenfold GTP. An extra 15% of ethylene glycol was used for cryo-protection. GTPγS-bound MFN1$_{IM}$A was crystallized in 0.1 M MIB (pH 6.0–8.0, PACT suite, QIAGEN), 25% PEG 1500 and directly flash-frozen in liquid nitrogen. Complex of MFN1$_{IM}$A with GDP was crystallized in approximately 50–80 mM sodium citrate and 23–25% PEG 3350 after a week. An extra 20% of MPD was used for cryo-protection. All crystals were stored in liquid nitrogen before diffraction assays. We also obtained crystals of apo MFN1$_{IM}$A and apo MFN1$_{IM}$B in conditions without nucleotides, but these crystals did not diffract X-ray well.

Structure determination. All diffraction datasets were collected at beamline BL17U1 of the Shanghai Synchrotron Radiation Facility (SSRF) and processed with the XDS suite[31]. Initial phases were calculated and refined by the single anomalous dispersion method using SHELXC/D/E[32] with the graphical interface HKL2MAP[33] from a diffraction data set of SeMet-substituted MFN1$_{IM}$B crystal in the apo form. Other structures were solved by molecular replacement using MolRep[34] and Phaser[35] with the structure of SeMet MFN1$_{IM}$B as the search model. Models were built with COOT[36] and refined with Refmac[37] and Phenix[38]. Structural validation was carried out using MolProbity[39]. Structural illustrations were prepared using the PyMOL Molecular Graphic Systems (version 0.99, Schrödinger LLC; http://www.pymol.org/). The 6.1 Å MFN1$_{IM}$A•GTPγS structure and 4.3 Å MFN1$_{IM}$A•GDP structure were not further refined after molecular replacement. X-ray data collection and refinement statistics can be found in Extended Data Table 1. The area of the G interface was calculated using the PISA server[40]. The Ramachandran statistics determined by PROCHECK[41] are as follows: 98.3% in favoured region, 1.7% allowed, 0 outlier for apo MFN1$_{IM}$B; 98.7% favoured, 1.0% allowed, 0.3% outlier for GTP-bound MFN1$_{IM}$C(T109A); 95.8% favoured, 4.1% allowed, 0.1% outlier for transition-like state MFN1$_{IM}$C and 98.0% favoured, 2.0% allowed, 0 outlier for GDP-bound MFN1$_{IM}$C(T109A).

RALS. A coupled RALS-refractive index detector (Malvern) was connected in line to an analytical gel filtration column Superdex200 10/300 to determine absolute molecular masses of the applied protein samples. For each experiment, 100 μM purified MFN1$_{IM}$C (wild type or mutants) or approximately 10–30 μM MFN1$_{\Delta TM}$ (wild type or mutants) was incubated with or without 1 mM corresponding ligand for 6 h at 25 °C before the measurement. The column was equilibrated with 20 mM HEPES, pH 7.2, 30 mM NaCl, 5 mM MgCl$_2$ and 1 mM DTT. Data were analysed with the provided OMNISEC software. All experiments were repeated at least twice and the data showed satisfying consistency.

GTP hydrolysis assay. GTP hydrolysis assays for MFN1$_{IM}$C, MFN1$_{\Delta TM}$ and corresponding mutants were carried out at 37 °C in 20 mM HEPES, pH 7.5, 150 mM NaCl, and 5 mM MgCl$_2$ and 1 mM DTT as described earlier[42]. For measuring stimulated GTP turnover of wild-type MFN1$_{IM}$C, MFN1$_{IM}$C(E209A), and MFN1$_{IM}$C(R238A), protein at concentrations of 0.5, 1, 2.5, 5, 10, 20 and 40 μM were individually mixed with 1–2 mM GTP and hydrolysis rates were determined from a linear fit to the initial rate of the reaction (<40% GTP hydrolysed). For other experiments, 20 μM protein and 1 mM GTP were used.

Nucleotide binding study. The equilibrium dissociation constants for MFN1$_{IM}$C and indicated mutants to guanine nucleotides were determined by isothermal titration calorimetry (ITC) using a MicroCal ITC200 (Malvern) at 25 °C. 2 mM nucleotide was titrated at 2 μl step against 60–80 μM protein in the buffer containing 20 mM HEPES, pH 7.5, 150 mM NaCl, 5 mM MgCl$_2$, 2.5 mM β-ME. Resulting heat changes upon each injection was integrated and the values were fitted to a standard single-site binding model using Origin7. All experiments were repeated at least twice and the data showed satisfying consistency.

Mitochondrial elongation assay. To examine the effect of point mutations, MFN1–Myc and MFN2–Myc variants were expressed in *Mfn1/2*-null MEFs from the pQCXIP retroviral vector. MEFs were generated in-house. The cell line is free of myoplasma and has been authenticated by genotyping with PCR to confirm deletion of the *Mfn1* and *Mfn2* genes. Point mutants in mouse *Mfn1* and *Mfn2* were constructed by overlapping PCR with primers encoding the point mutation. All mutations were confirmed by DNA sequencing. The types and positions of the residues mutated in this study are all consistent between human and mouse mitofusins. Retroviral supernatants were produced from 293T cells transfected with the retroviral vector and the packaging plasmid pCLEco. *Mfn1/2*-null MEFs were maintained in DMEM supplemented with 10% fetal bovine serum and penicillin/streptomycin at 37 °C and 5% CO$_2$. After retroviral transduction of *Mfn1/2*-null MEFs, puromycin selection was applied for 2 days. Cells were plated onto 8-well chambered slides for analysis. In the case of *Mfn1* constructs, *Mfn1/2*-null cells stably expressing mito-DsRed were used; for *Mfn2* constructs, *Mfn1/2*-null cells stably expressing mito-eGFP were used. Immunostaining and western blot analysis with the 9E10 antibody against Myc was performed to confirm localization and proper expression of the mitofusin variant. Mitochondrial morphology was scored by analysis of mito-DsRed or mito-GFP as described previously[12].

Liposome tethering assay. POPC (1-palmitoyl-2-oleyl-*sn*-glycero-3-phosphocholine), DOPS (1,2-dioleyl-*sn*-glycero-3-phospho-L-serine), DOGS-NTA-Ni^{2+} (1,2-dioleoyl-*sn*-glycero-3-[(*N*-(5-amino-1-carboxypentyl)iminodiacetic acid) succinyl] (nickel salt)) and Rho-DPPE (1,2-dipalmitoyl-*sn*-glycero-3-phosphoethanolamine-*N*-(lissamine rhodamine B sulfonyl)) (Avanti Polar Lipids) were mixed in a molar ratio of 78.5:15:5:1.5. Lipid film formed by evaporating chloroform under mild nitrogen stream was dehydrated in a vacuum drier before being re-suspended in buffer L (20 mM HEPES, pH 7.5, 150 mM NaCl, 2 mM β-ME) to a final concentration of 10 mM. Liposomes were prepared as previously described[30]. An internal His$_{12}$ tag was inserted between α3^H and α4^H of MFN1$_{IM}$C and corresponding mutants. For each reaction, 0.5 μM protein was mixed with 1 mM prepared liposomes in buffer L for 30 min at 4 °C before 5 mM GTP or GTPγS was subsequently added. After incubation for another 40 min at 37 °C, the proteoliposomes were imaged by a fluorescent microscope. Otherwise, the proteoliposomes were incubated with 300 mM imidazole, pH 7.5, for another 20 min to release the protein and then imaged. All experiments were repeated at least twice and the data showed satisfying consistency.

Data availability. The X-ray crystallographic coordinates and structure factor files for MFN1$_{IM}$ structures have been deposited in the Protein Data Bank (PDB) under the following accession numbers: 5GO4 (apo MFN1$_{IM}$B), 5GOF (GTP-bound MFN1$_{IM}$C(T109A)), 5GOM (transition-like state MFN1$_{IM}$C), and 5GOE (GDP-bound MFN1$_{IM}$C(T109A)). All other data generated or analysed during this study are included in this published article, and are available from the corresponding author upon reasonable request.

31. Kabsch, W. Xds. *Acta Crystallogr. D* **66,** 125–132 (2010).
32. Sheldrick, G. M. A short history of SHELX. *Acta Crystallogr. A* **64,** 112–122 (2008).
33. Pape, T. & Schneider, T. R. *HKL2MAP*: a graphical user interface for macromolecular phasing with *SHELX* programs. *J. Appl. Crystallogr.* **37,** 843–844 (2004).
34. Vagin, A. & Teplyakov, A. *MOLREP*: an automated program for molecular replacement. *J. Appl. Crystallogr.* **30,** 1022–1025 (1997).
35. McCoy, A. J. *et al.* Phaser crystallographic software. *J. Appl. Crystallogr.* **40,** 658–674 (2007).
36. Emsley, P. & Cowtan, K. Coot: model-building tools for molecular graphics. *Acta Crystallogr. D* **60,** 2126–2132 (2004).
37. Murshudov, G. N., Vagin, A. A. & Dodson, E. J. Refinement of macromolecular structures by the maximum-likelihood method. *Acta Crystallogr. D* **53,** 240–255 (1997).
38. Adams, P. D. *et al.* PHENIX: a comprehensive Python-based system for macromolecular structure solution. *Acta Crystallogr. D* **66,** 213–221 (2010).
39. Chen, V. B. *et al.* MolProbity: all-atom structure validation for macromolecular crystallography. *Acta Crystallogr. D* **66,** 12–21 (2010).
40. Krissinel, E. & Henrick, K. Inference of macromolecular assemblies from crystalline state. *J. Mol. Biol.* **372,** 774–797 (2007).
41. Laskowski, R. A., MacArthur, M. W., Moss, D. S. & Thornton, J. M. *PROCHECK*: a program to check the stereochemical quality of protein structures. *J. Appl. Crystallogr.* **26,** 283–291 (1993).
42. Gao, S. *et al.* Structural basis of oligomerization in the stalk region of dynamin-like MxA. *Nature* **465,** 502–506 (2010).
43. Thompson, J. D., Higgins, D. G. & Gibson, T. J. CLUSTAL W: improving the sensitivity of progressive multiple sequence alignment through sequence weighting, position-specific gap penalties and weight matrix choice. *Nucleic Acids Res.* **22,** 4673–4680 (1994).
44. Kelley, L. A., Mezulis, S., Yates, C. M., Wass, M. N. & Sternberg, M. J. The Phyre2 web portal for protein modeling, prediction and analysis. *Nat. Protocols* **10,** 845–858 (2015).
45. Prakash, B., Praefcke, G. J., Renault, L., Wittinghofer, A. & Herrmann, C. Structure of human guanylate-binding protein 1 representing a unique class of GTP-binding proteins. *Nature* **403,** 567–571 (2000).
46. Fröhlich, C. *et al.* Structural insights into oligomerization and mitochondrial remodelling of dynamin 1-like protein. *EMBO J.* **32,** 1280–1292 (2013).
47. Brandt, T., Cavellini, L., Kühlbrandt, W. & Cohen, M. M. A mitofusin-dependent docking ring complex triggers mitochondrial fusion in vitro. *eLife* **5,** e14618 (2016).
48. McMahon, H. T., Kozlov, M. M. & Martens, S. Membrane curvature in synaptic vesicle fusion and beyond. *Cell* **140,** 601–605 (2010).
49. Richard, J. P. *et al.* Intracellular curvature-generating proteins in cell-to-cell fusion. *Biochem. J.* **440,** 185–193 (2011).
50. Stachowiak, J. C. *et al.* Membrane bending by protein-protein crowding. *Nat. Cell Biol.* **14,** 944–949 (2012).
51. Kozlov, M. M. *et al.* Mechanisms shaping cell membranes. *Curr. Opin. Cell Biol.* **29,** 53–60 (2014).
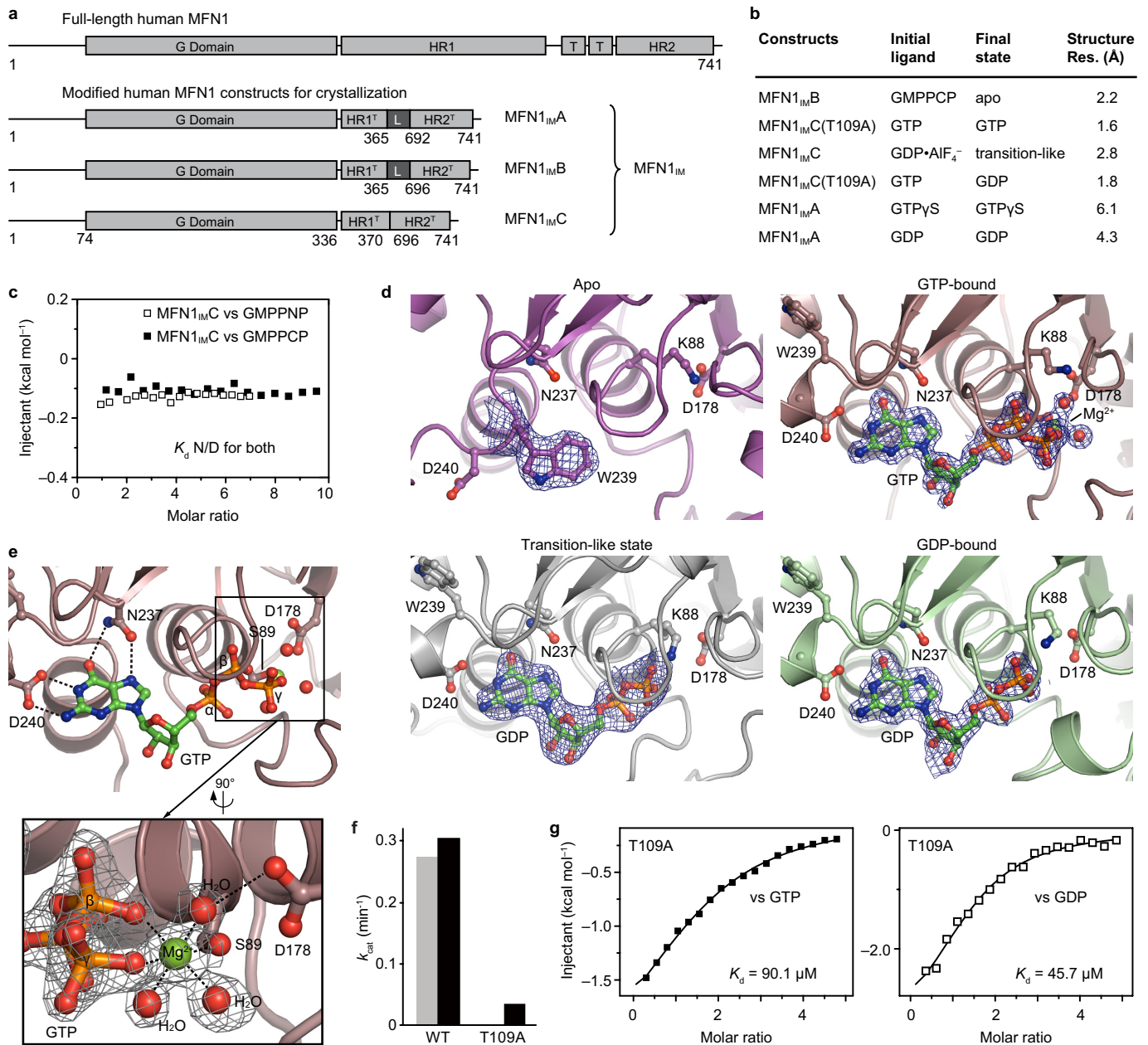
Extended Data Figure 1 | MFN1 constructs and their biochemical properties. **a**, Schematic representation showing the strategy of generating human MFN1 constructs for crystallization. Indication of the labels and numbers are the same as in Fig. 1a. $HR1^T$ and $HR2^T$ denote truncated HR1 and HR2, respectively. We removed the transmembrane (TM) region and flanking residues from human MFN1 and inserted artificial linkers as illustrated. Three different constructs used for crystallization are named $MFN1_{IM}A$, $MFN1_{IM}B$ and $MFN1_{IM}C$, respectively (collectively termed $MFN1_{IM}$). **b**, Summary of the crystal structures. 'Initial ligands' denotes ligands added to the protein solution before crystallization, whereas 'final state' denotes the contents from the refined structure. Resolutions for the structure are specified. **c**, ITC results showing that $MFN1_{IM}$ constructs have no binding affinity to GMPPNP or GMPPCP. Only the result of the $MFN1_{IM}C$ construct is shown here as representative. **d**, Electron density of the guanine nucleotides in corresponding structures. The electron density maps are all shown at a contour level of 1.2σ. The residues involved in ligand coordination are shown as ball-and-stick models. **e**, Details of the $MFN1_{IM}$ active site in the GTP-bound state. Key hydrogen bonds for coordinating the GTP were indicated by dotted lines. In the bottom panel, details of the Mg^{2+} coordination is depicted. The electron density for Mg^{2+} ion, water and GTP was shown as grey mesh at a contour level of 1.2σ. **f**, GTP turnover rates of wild-type $MFN1_{IM}$ and $MFN1_{IM}(T109A)$. $MFN1_{IM}(T109A)$ shows greatly impaired GTPase activity that facilitates the co-crystallization with GTP. Results from two separated experiments are presented for each protein. **g**, ITC results showing that $MFN1_{IM}(T109A)$ binds both GTP and GDP.
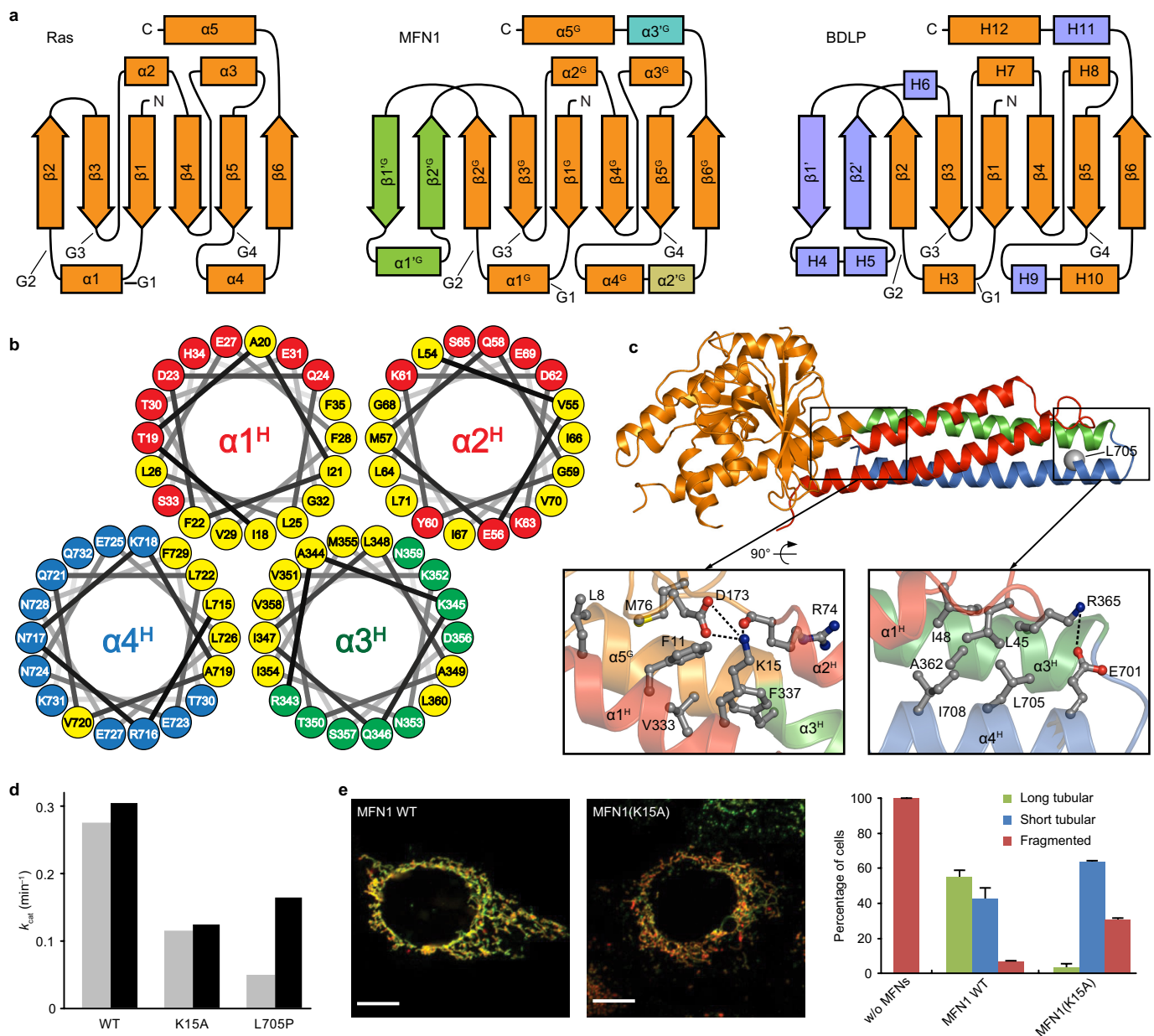
Extended Data Figure 2 | Overall structure of MFN1$_{IM}$. a, The topology diagrams of the G domains of Ras, MFN1 and BDLP. Secondary structural elements were not drawn to scale and positions of G1–G4 motifs are indicated. Elements of MFN1 are named and coloured as in Fig. 1c. For BDLP, elements extra than Ras in light blue. The helices of BDLP are named as in ref. 21. **b**, Helical wheel diagrams of HD1. Hydrophobic residues are coloured yellow and other residues are coloured with the corresponding helices as in Fig. 1d. The plots are arranged according to the positions of the four helices of HD1 in the crystal structure, showing a massive hydrophobic core of HD1. **c**, Intramolecular association of MFN1$_{IM}$. For the G-domain–HD1 interaction, Leu8, Met76, Val333 and Phe337 embrace Phe11, whereas Lys15 forms a salt bridge with Asp173 and a hydrogen bond with the main chain oxygen of Arg74. The MFN1(L705P) mutant was previously found to be non-functional in mediating mitochondrial fusion[13]. Leu705 is surrounded by several hydrophobic residues including Ile45, Ile48, Ala362 and Ile708, as well

as a salt bridge formed by Arg365 and Glu701. The proline mutation of Leu705 may disrupt α4^H and the local hydrophobic interactions, thereby impeding the folding of the protein. **d**, GTP turnover rates of wild-type MFN1$_{IM}$ and MFN1$_{IM}$(K15A) and MFN1$_{IM}$(L705P). Results from two separated experiments are presented for each protein. **e**, Mitochondria elongation assays of wild-type MFN1 and MFN1(K15A). The Myc-tagged MFN1 constructs were assayed for mitochondrial elongation activity by expression in *Mfn1/2*-null MEFs, which have completely fragmented mitochondria. Overexpression of wild-type MFN1 in *Mfn1/2*-null MEFs induces the formation of mostly tubular mitochondria, indicating normal elongation activity, whereas MFN1(K15A) induces substantially less mitochondrial tubulation. Green fluorescence is from immunostaining against the Myc epitope; red fluorescence is from mito-DsRed. The data are quantified on the right. For each construct, 100 cells were scored in biological triplicate; representative images are shown. Error bars indicate s.e.m. Scale bars, 10 μm.

```
                                                                                      α1^H
                                                                              ◆◆  ◆ ◆    ◆
hsMFN1  ---------- ---------- ---------- ---------- ---------- ----------  -    hsMFN1  -----MAEPV SPLKHFVLAK KAITAIFDQL LEFVTEGSHF VEATYKNPEL DRIATEDDLV  55
hsMFN2  ---------- ---------- ---------- ---------- ----MSLLFS RCNSIVTVKK  16   hsMFN2  NKRHMAEVNA SPLKHFVTAK KKINGIFEQL GAYIQESATF LEDTYRNAEL DPVTTEEQVL  76
mmMFN1  ---------- ---------- ---------- ---------- ---------- ----------  -    mmMFN1  -----MAETV SPLKHFVLAK KAITAIFGQL LEFVTEGSHF VEATYRNPEL DRIASEDDLV  55
mmMFN2  ---------- ---------- ---------- ---------- ----MSLLFS RCNSIVTVKK  16   mmMFN2  DKRHMAEVNA SPLKHFVTAK KKINGIFEQL GAYIQESASF LEDTHRNTEL DPVTTEEQVL  76
dmMarf  MAAYLNRTIS MVTGQTGPAD DDRHASSTDT VDKSGPGSPL SRFNSSLQQS GSTMAANLLP  60   dmMarf  ESRLYQSNDK SPLQIFVRAK KKINDIYGEI EEYVHETTTF INALHAEAEI VDKAER---E 117
dmFzo   ---------- ---------- ---------- ---------- --------MA ESDSGESTSS  12   dmFzo   VSSFISSSSS SRLSEFVDAK TELQDIYHDL SNYLSNFLTI LEETVLLK-- ----DRQMLE  66
BDLP    ---------- ---------- ---------- ---------- ---------- ----------  -    BDLP    ------MVNQ VATDRFIQDL ERVAQVRSEM SVCLNKLAET INKAELAGD- ----SSSGKL  49
                                                                                                    H1
```

```
         α2^d          β1^G       α1^G          β2^G                                       β1           α1'^G          β2
                  G1            ◆    ◆   ● G2                                                      ▲▲
hsMFN1  EMQGYKDKLS IIGEVLSRRH MKVAFFGRTS SGKSSVINAM LWDKVLPSGI GHITNCFLSV 115   hsMFN1  EGTDGDKAYL MTEGSDEK-- ------KSVK TVNQLAHALH MDKDLKAGCL VRVFVWPKAKC 167
hsMFN2  DVKGYLSKVR GISEVLARRH MKVAFFGRTS NGKSSVINAM LWDKVLPSGI GHTTNCFLRV 136   hsMFN2  EGTDGHEAFL LTEGSEEK-- ------RSAK TVNQLAHALH QDKQLHAGSL VSVMWPNSKC 188
mmMFN1  EIQGYRNKLA VIGEVLSRRH MKVAFFGRTS SGKSSVINAM LWDKVLPSGI GHITNCFLSV 115   mmMFN1  EGTDGDKAYL MTEGSDEK-- ------KSVK TVNQLAHALH MDKDLKAGCL VHVFVWPKAKC 167
mmMFN2  DVKGYLSKVR GISEVLARRH MKVAFFGRTS NGKSSVINAM LWDKVLPSGI GHTTNCFLRV 136   mmMFN2  EGTDGHEAFL LTEGSEEK-- ------KSVK TVNQLAHALH QDEQLHAGSM VSVMWPNSKC 188
dmMarf  LFESYYKVA AIREVLQRDH MKVAFFGRTS SGKSSVINAM LREKILPSGI GHTTNCFCQV 177    dmMarf  EGSNGGEAYL MTEGSEEK-- ------LNVV NIKQLANALC QEKLCES-SL VRIFWPRERC 228
dmFzo   HLCAFSSRVE AIAKVLSRDR MKVAFFGRTS NGKSAVINAL LHEKILPSAM GHTTSCFCQV 126   dmFzo   QANGSNETEH VKVEQEDE-- ------HMEL SALSQLASAH SPGALKPSTL LQVNMAKNRC 178
BDLP    SLERDIEDIT IASKNLQQGV FRLLVLGDMK RGKSTFLNAL IGENLLPSDV NPCTAVLTVL 109   BDLP    RYGPEKKVTI HFNDGKSPQQ LDFQNFKYKY TIDPAEAKKL EQEKKQAFPD VDYAVVEYPL 169
          H2          β1         H3          β2                                              β3          H4         H5          β4
```

```
         β3^G          α2^G         β4^G           α3^G                                     β5^G           α4^G          α2'^G β6^G
              G3                 ■              ▲                                              G4      ▲ ▲        ▲
hsMFN1  ALLRDDLVLV DSPGTDVTTE LDSWIDKFCL DADVFVLVAN SESTLMNTEK HFFHKVNERL 227   hsMFN1  SKPNIFILNN RWDAS-ASEP E----YMEDV RRQHMERCLH FLVEELKVV- NALEAQNRIF 281
hsMFN2  PLLRDDLVLV DSPGIDVTTE LDSWIDKFCL DADVFVLVAN SESTLMQTEK HFFHKVSERL 248   hsMFN2  SRPNIFILNN RWDAS-ASEP E----YMEDV RRQHMERCTS FLVDELGVV- DRSQAGDRIF 302
mmMFN1  ALLRDDLVLV DSPGTDVTTE LDIWIDKFCL DADVFVLVAN SESTLMNTEK HFFHKVNERL 227   mmMFN1  SKPNIFILNN RWDAS-ASEP E----YMEDV RRQHMERCLH FLVEELKVV- SPSEARNRIF 281
mmMFN2  PLLRDDLVLV DSPGIDVTTE LDSWIDKFCL DADVFVLVAN SESTLMQTEK HFFHKVSERL 248   mmMFN2  SRPNIFILNN RWDAS-ASEP E----YMEDV RRQHMERCTS FLVDELGVV- DRAQAGDRIF 302
dmMarf  SLLRDDVVFV DSPGVDVSAN LDDWIDNHCL NADVFVLVLN AESTMTRAEK QFFHTVSQKL 288   dmMarf  SKPNIFILNN RWDAS-ANEP E----CQESV KSQHTERCID FLTKELKVS- NEKEAAERVF 342
dmFzo   SILDYDVVLM DTPGVDVTAQ LDDCLDSYCM DADVFILVLN AESTVSRVER QFFKDVASKL 238   dmFzo   SRPNLFILNN RWDKASSLEP E----MEQKV KDQHMERCVN LLVDELGVYS TAQEAWERIY 294
BDLP    TLLQKGIEIV DSPGLNDTEA RNELSLGYVN NCHAILFVMR ASQPCTLGER RYLENYIKGR 229   BDLP    G-LTVFFLVN AWDQVRESLI DPDDVEELQA SENRLRQVFN ANLAEYCTVE GQNIYDERVF 288
           H6  β5        H7          β6         H8                                            β7  H9        H10         β8
```

```
              α3'^G          α5^G                                          Artifitial  Predicted Secondary Structure
                                                                           linker
                       ▲                                                 ◆ ◆◆  ◆   ◆
hsMFN1  FVSAKEVLSA RKQKAQGMPE SGVALAEGFH ARLQEFQNFE QIFEECISQS AVKTKFEQHT 341   hsMFN1  IRAKQILATV KNIMDS-VNL AAEDKRHYSV EEREDQIDRL DFIRNQMNLL TLDVKKKIKE 400
hsMFN2  FVSAKEVLNA RIQKAQGMPE GGGALAEGFQ VRMFEFQNFE RRFEECISQS AVKTKFEQHT 362   hsMFN2  VRAKQIAEAV RLIMDS-LHM AAREQQVYCE EMREERQDRL KFIDKQLELL AQDVKLRIKQ 421
mmMFN1  FVSAKEVLNS RKHKAQGMPE GGGALAEGFQ VRMFEFQNFE RQFEECISQS AVKTKFEQHT 341   mmMFN1  IRAKQILDTV KNILDS-VNV AAEKRVYSM EMREERQDRL DFIRNQMNLL TLDVKKKIKE 400
mmMFN2  FVSAKEVLNA RVQKAQGMPE GGGALAEGFQ VRMFEFQNFE RQFEECISQS AVKTKFEQHT 362   mmMFN2  VRAKQIAEAV RLIMDS-LHI AAQEQRVYCL EMREERQDRL KFIDKQLELL AQDVKLRIKQ 421
dmMarf  FVSARETLQA RIEEAKGNPP HMGAIAEGFQ IRYFEFQDFE KFEECISQS AVKTKFQQHT 402    dmMarf  SRGKSVSGDM KSMLDN-IYE RITIFRNLKQ DQKNLLTERI QGTETQMMQV TREMKMKIHN 461
dmFzo   HVSALEALHI RNGQIT-NP- -----SGQTQ QRYQEFLRFE NDFSNCLAVS ALKTKFGPHL 347   dmFzo   LSAQKILNQL KSTLICPFIE KVSRLIDENK ERRANLNAEI EDWLILMQED REALQYCFEE 407
BDLP    ELSSIQALRR RLK----NP- -QADL-DTG -----FPKFM DSLNTFLTRE RAIALRLQVR 336   BDLP    TLARLACNHT REAVAR---- -RIPLLEQDV NELKKRIDSV EPEFNKLTGI RDEFQKEIIN 391
           H11         H12        H13                                                H13             H14
```

```
hsMFN1  VTEEVANKVS CAMTDEICRL S-VLVDEFCS EFHPNPDVLK IYKSELNKHI EDGMGRNLAD 459   hsMFN1  RCTDEVNALV LQTQQEIIEN LKPLLPAG-- IQDKLHTLIP CKKFDLSYNL NYHKLCSDFQ 517
hsMFN2  ITEEVERQVS TAMAEEIRRL S-VLVDDYQM DFHPSPVVLK VYKNELHRHI EEGLGRNMSD 480   hsMFN2  RCSTAITNSL QTMQQDMIDG LKPLLPVS-- VRSQIDMLVP RQCFSLNYDL NCDKLCADFQ 538
mmMFN1  VTEEVANKVS CAMTDEICRL S-VLVDEFCS EFHPTPSVLK VYKSELNKHI EDGMGRNLAD 459   mmMFN1  RCTNEVNASI LQSQQEIIEN LKPLLPVS-- IQNKLHTLIP CKKFDLSYNL NCDKLCSDFQ 517
mmMFN2  ITEEVERQVS TAMAEEIRRL S-VLVDEYQM DFHPSPVVLK VYKSELHRHI EEGLGRNLSD 480   mmMFN2  RCSTAIASSL QTMQQDMIDG LKPLLPVS-- MRNQIDMLVP RQCFSLSYDL NCDKLCADFQ 538
dmMarf  MVEEVEEKVS KALNEEIWRL G-VLVDEFNM DFHPERLVLN IYKKELNAHV ESGLGSNLRA 520   dmMarf  RLSMALAMNV ESAQTEMTDR MHALVPNEQL LATSTKMVVR TQPFEMLYSL NCQNLCADFQ 580
dmFzo   LTEMTQRVGR CVLNDQIKTL IPSSVLSFSQ PFHP---EFP AQIGQYQRSL CAHLDKLLED 464   dmFzo   RVLQCLSIPL QRKILDIEKE IGLPIAEN-- ---------- SCDWQLIYGL DCQSYMSDFQ 512
BDLP    TRDTQARTIS ESFRSYVLNL G-NTFENDFL RYQPELNLFD FLSSGKREAF NAALQKAFEQ 450   BDLP    YITDKSAAWT LTAEKDINAA FKELSRSA-- ---------- SQYGASYNQI TDQITEKLTG 498
           H14        H15    H16       H17                                                    H18
```

```
hsMFN1  EDIVPPFSLG WSSLVHRFLG PRNAQ----- ----RVLLG LSEPIFQLPR SLASTPTAPT 567   hsMFN1  TPATPDNASQ EELMITLVTG LASVTSRTSM GIIIVGGVIW KTIGWKLLSV SLTMYGALYL 627
hsMFN2  EDIEFHFSLG WTMLVNRFLG PKNSR----- ----RALMG YNDQVQRPIP LTPANPSMP- 587   hsMFN2  -PLPQGSLTQ EEFMVSMVTG LASLTSRTSM GILVVGGVVW KAVGWRLIAL SFGLYGLLYV 646
mmMFN1  EDIVFHFSLG WSSLVHRFLG STNAQ----- ----RVLLG LSEPIFQLPR SLASTPTAPS 567   mmMFN1  NPAAPDNAAQ EELMITLTG LASLTSRTSM GIIVVGGVIW KTVGWKLISV TLSMYGALYL 627
mmMFN2  EDIEFHFSLG WTMLVNRFLG PKNSR----- ----RALLG YSDQVQRPLP LTPANPSMP- 587   mmMFN2  -PLPQSSLTQ EELMVSMVTG LASLTSRTSM GILVVGGVVW KAVGWRLIAL SFGLYGLLYV 646
dmMarf  EDLEKFWTNSA IAAMIQRFTG KVRERSKKGQ PALVNRQSSI GHSVSTPTTT PVEATPVCLL 640   dmMarf  PAPVVAGITP EQLSLISRFA VSSIGSGGTV GGLVVAGVML KTIGWRVLVG VGALYGCIYL 700
dmFzo   PDLRFRFSLG FTALWHRLEG N--------- ------LP LHASPFRIQK LQNGHKKCSP 555    dmFzo   LPPLVNGNHW QMLESLVKS- ------KGSL GTVLLSAMAI RSFNWPIVLL LGGLVGSFYI 608
BDLP    KDVKVHTTTT AEEDNS---- ---------- ---------- PGWAKWAMGL LSLSKGNLAG 534   BDLP    FALAGAGFDW KNILLNYFTV IG-----IGG IITAVTGILL GPIGFALLGL GVGFLQADQA 589
                              H19                                                                   H20
```

```
                                                                           Predicted S. S.                α4^H
                                                                                          ◆  ◆◆    ◆
hsMFN1  YERLSWTTHA KERAFKQQFV NYATEKLRMI VSSTSANCSH QVKQQIATTF ARLCQQVDIT 687   hsMFN1  QKQLEEEIAR LPKEIDQLEK IQNNSKLLRN KAVQLENELE NFTKQFLPSS NEES 741
hsMFN2  YERLTWTTKA KERAFKRQFV EHASEKLQLV ISYTGSNCSH QVVQQELSGTF AHLCQQVDVT 706   hsMFN2  RENLEQEIAA MNKKIEVLDS LQSKAKLLRN KAGWLDSELN MFTHQYLQPS R--- 757
mmMFN1  YERLTWTTHA KERAFKKQFV NYATEKLQMI VSSTSANCSH QVVQEMATTF ARLCQQVDIT 687   mmMFN1  QKHLEEEIAR LSKEIDQLEK IQNNSKLLRN KAVQLENELE NFSKQFLHPS SGES 741
mmMFN2  YERLTWTTKA KERAFKRQFV EYASEKLQLI ISYTGSNCSH QVVQQELSGTF AHLCQQVDVT 706   mmMFN2  RDNLEQEIAA MNKKVEALDS LQSRAKLLRN KAGWLDSELN MFTHQYLQPS R--- 757
dmMarf  YERLSWTNSA KERTFKSQYA RHATKKLKNI QNGLNSATCSH QVVQQELSSTF ARLCRTVDTA 760   dmMarf  TTDMNDELKT LDSQLNILEA NQKQLKLLRN KANYIQNELD IFEHNYISPQ ---- 810
dmFzo   YEYAAWTTAA QERSFKSQYA RLLQQRLRSD VQQTVSGFEL QLRQHLATVR NCWEAQSNET 668   dmFzo   LNDLNVRTAE LTKQIQSMEV LQLSLKKFRD KGQLLASRLG DFQETYLTKS ---- 718
BDLP    RRELVKTAKK ELVKHLPQVA HEQSQVVYNA VKECFDSYER EVSKRINDDI VSRKSELDNL 649   BDLP    VKQKQTREIN RESEFNRLKN LQEDVIAQLQ KIEAAYSNLL AYYS------ ---- 693
                                  H21                                                                  H22
```

Extended Data Figure 3 | Sequence alignment of mitofusins and BDLP.
Sequence alignment of mitofusins and BDLP. Amino acid sequences of human (hs) MFN1 (UniProt accession Q8IWA4) and MFN2 (O95140), mouse (mm) MFN1 (Q811U4) and MFN2 (Q80U63), fruitfly (*Drosophila melanogaster*, dm) Marf (Q7YU24), fruitfly Fzo (O18412) and BDLP from *N. punctiforme* (B2IZD3) are aligned using Clustal W[43]. Residues with a conservation of 100% are in red shades, greater than 80% in green shades and 50% in grey shades, respectively. α-helices are shown as cylinders and β-strands as arrows for both nucleotide-free human MFN1 (above the sequences) and nucleotide-free BDLP (2J, under the sequences). In the case of human MFN1, the secondary structure signs are coloured as in

Fig. 1b and labelled as in Fig. 1b–d for MFN1$_{IM}$ regions. Secondary structural elements of the missing HD2 and transmembrane domain predicted from the PHYRE2 server[44] (exclusively α-helices) are depicted as shaded cylinders with dashed outlines. For BDLP, the secondary structure signs are coloured grey and labelled according to the previous report[21]. The G1–G4 elements are specified in the sequences. Key residues on human MFN1 are also indicated, including those involved in the hydrophobic core of HD1 (diamond symbol), hinges (downwards triangle), guanine nucleotide binding and hydrolysis (circle), G interface (upwards triangle), and the plausible HD1–HD2 conformational change (square).
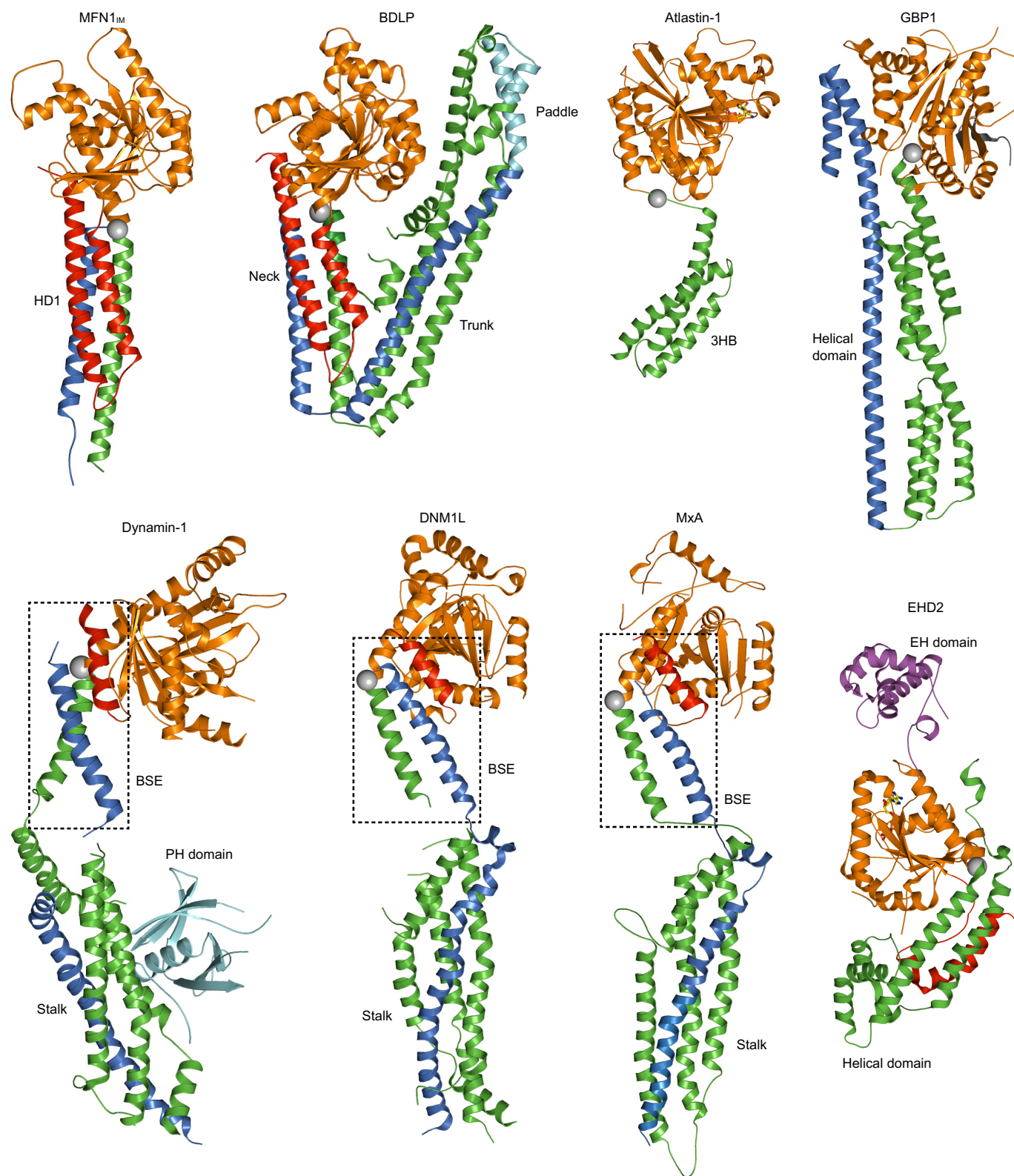
Extended Data Figure 4 | Structural comparison of MFN1$_{IM}$ with other dynamin family members. Structural comparison of nucleotide-free MFN1$_{IM}$B with nucleotide-free BDLP (PDB code 2J69)[21], GDP-bound atlastin-1 (3Q5D)[19], nucleotide-free GBP1 (1DG3)[45], nucleotide-free dynamin-1 (3SNH)[17], nucleotide-free DNM1L (4BEJ)[46], nucleotide-free MxA (3SZR)[16], and AMPPNP-bound EHD2 (2QPT)[15]. For these molecules, the region N-terminal to the G domain is in red, the G domain itself in orange, the conventional middle domain is in green, the conventional GTPase effector domain (GED) in marine, the paddle region of BDLP and the pleckstrin homology (PH) domain of dynamin-1 is in cyan, and the Eps15 homology (EH) domain of EHD2 is in magenta. The hinges between the G domains and middle domains are depicted by grey spheres. Nucleotides are shown as ball-and-stick models.
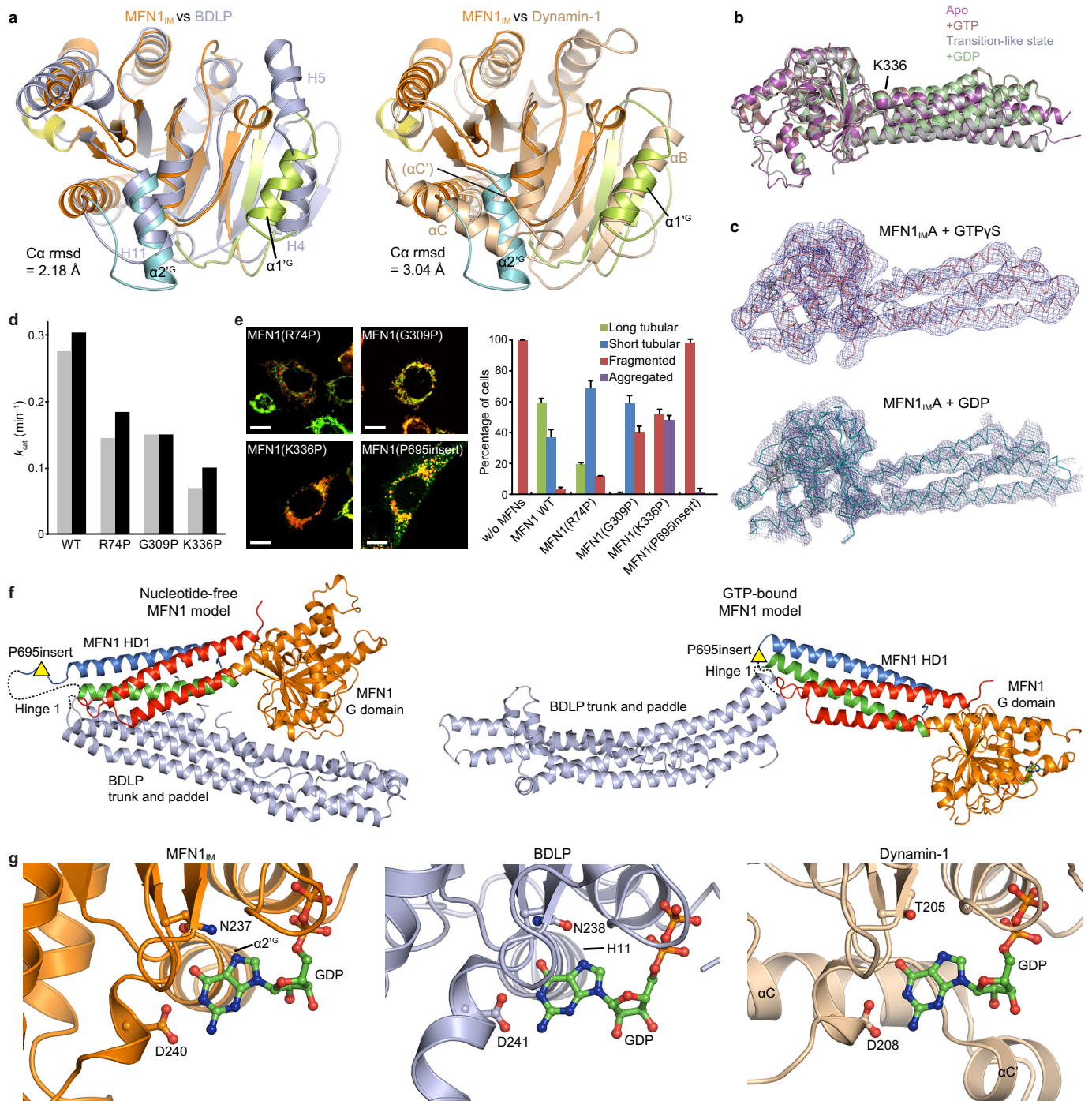
Extended Data Figure 5 | Structural comparison of MFN1$_{IM}$ with BDLP and dynamin-1. a, Structural comparison of the G domains between MFN1$_{IM}$ and BDLP (left) or dynamin-1 (right) in the nucleotide-free state. The MFN1 G domain (coloured as in Fig. 1b) is separately superimposed with G domains of BDLP (PDB code 2J69, light blue) and rat dynamin-1 (2AKA, wheat). The root mean standard deviation (r.m.s.d.) values of aligned Cα atoms are shown. α-helices on the two lobes are labelled. The G domain of MFN1$_{IM}$ resembles the BDLP G domain, except that at lobe 1, dynamin-1 is similar to MFN1$_{IM}$ in lobe 1, but at lobe 2 the αC tilts 60° from its counterpart α2'^{G} in MFN1$_{IM}$. **b**, Structural comparison of MFN1$_{IM}$ in different nucleotide-loading states. Structures of nucleotide-free MFN1$_{IM}$B, GTP-bound MFN1$_{IM}$C(T109A), transition-like state MFN1$_{IM}$C and GDP-bound MFN1$_{IM}$C(T109A) are colour-specified and superimposed on their G domains. **c**, Architectures of MFN1$_{IM}$A•GTPγS and MFN1$_{IM}$A•GDP. Shown are the corresponding Cα traces and electron density maps (contoured at 1.2σ), by which molecule outlines are clearly discernible. These two structures are presented to exclude possible influence of the Thr109Ala mutation in

the GTP- and GDP-bound structures shown in **b**. **d**, GTP turnover rates of wild-type MFN1$_{IM}$ and the hinge 2 mutants. Results from two experiments are shown for each protein. **e**, Mitochondrial elongation assay for wild-type MFN1 and the hinge mutants. For each construct, 100 cells were scored in biological triplicate; representative images are shown. Error bars indicate s.e.m. Scale bars, 10 μm. **f**, Full-length MFN1 models showing the plausible hinge 1 between HD1 and HD2. Models were based on nucleotide-free (PDB code 2J69, top) and GMPPNP-bound (2W6D, bottom) BDLP. G domain and HD1 are coloured as in Fig. 1b; HD2 is in light blue. Hinge 1 is shown as dashed lines. Yellow triangles indicate approximate position for the Pro695 insert. **g**, Extra support of the guanine base in MFN1 (GDP-bound MFN1$_{IM}$C(T109A), coloured as in Fig. 1c), BDLP (PDB code 2J68, light blue) and dynamin-1 (5D3Q, wheat). The α-helices that support the guanine base are specified. Parts of the G domains are removed for clarity. Note the similarity between MFN1$_{IM}$ and BDLP, as well as the difference between MFN1$_{IM}$ and dynamin-1 in nucleotide coordination.
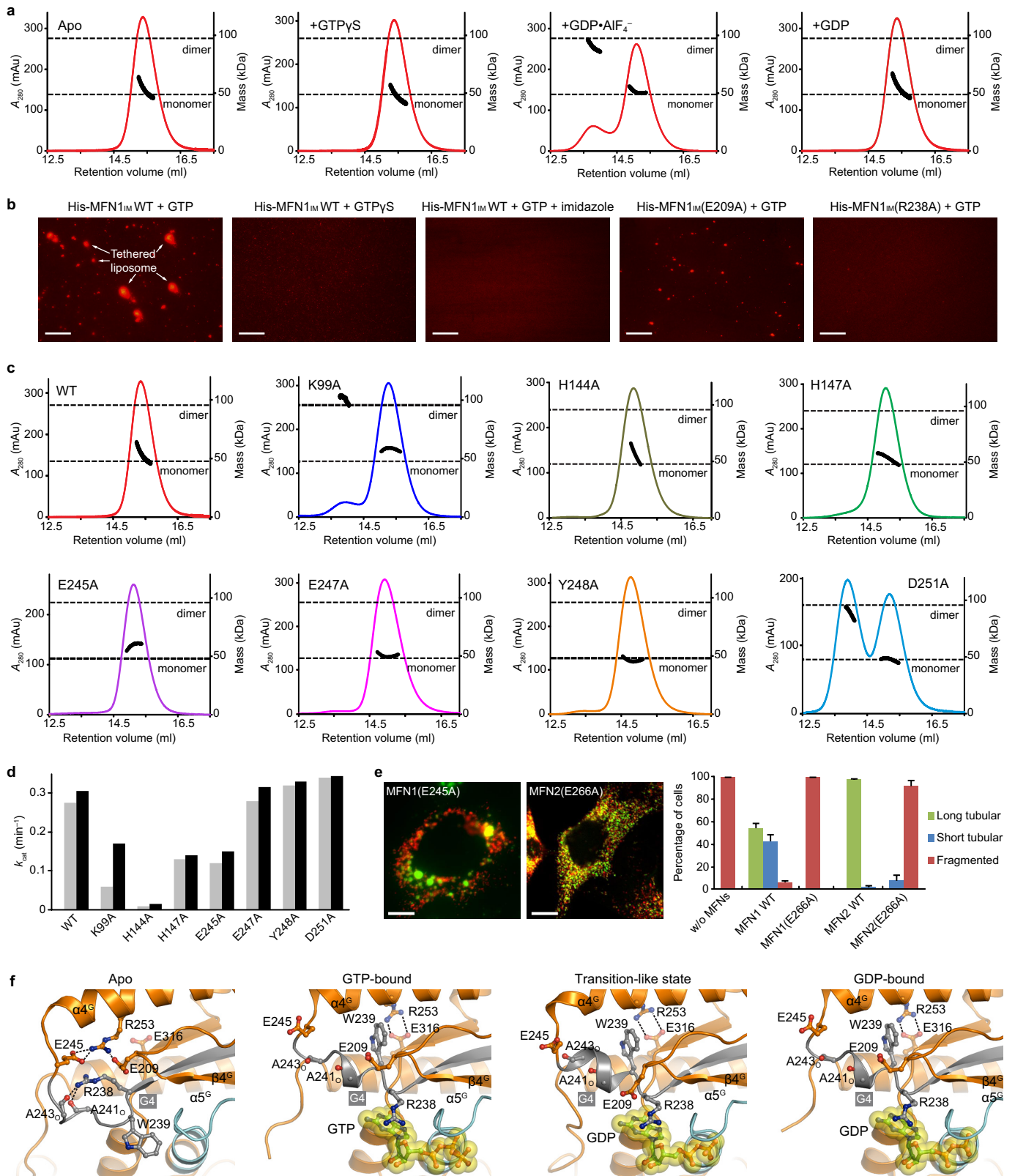
Extended Data Figure 6 | See next page for caption.

Extended Data Figure 6 | Dimerization of MFN1$_{IM}$ G domains in the transition-like state. a, Oligomerization states of MFN1$_{IM}$ in different nucleotide-loading conditions by RALS. MFN1$_{IM}$ is monomeric in nucleotide-free, GTPγS-bound and GDP-bound states, and forms dimers in the presence of GDP•AlF$_4^-$. Data are as in Fig. 3d. **b**, Liposome tethering assay for wild-type MFN1$_{IM}$ and corresponding mutants. Representative images from five separate experiments are shown. Wild-type MFN1$_{IM}$ tethered liposomes carrying fluorescence in the presence of GTP hydrolysis-dependent manner as large aggregated liposomes were observed (first left). In GTPγS-present condition the liposome aggregation was largely attenuated, suggesting that tethering is dependent on GTP hydrolysis (second left). When proteins were washed off the liposome by imidazole, the liposomes became homogeneously scattered (middle), indicating that the liposomes were tethered but did not merger. MFN1$_{IM}$(E209A) and MFN1$_{IM}$(R238A) displayed suppressed tethering activity (right two). Scale bars, 50 μM. **c**, Dimerization test of the G interface mutants in the presence of GDP•AlF$_4^-$. **d**, GTP turnover rates of the G interface mutants compared with wild-type MFN1$_{IM}$. Results from two separated experiments are presented for each protein. **e**, Mitochondrial elongation assay for MFN1(E245A) and related MFN2(E266A). For each construct, 100 cells were scored in biological triplicate; representative images are shown. Error bars indicate s.e.m. Scale bars, 10 μm. Both mutants lost fusogenic activity. **f**, Rearrangement of residues in the G interface upon nucleotide binding. Structures shown from left to right are: nucleotide-free MFN1$_{IM}$B; GTP-bound MFN1$_{IM}$C(T109A); transition-like state MFN1$_{IM}$C; and GDP-bound MFN1$_{IM}$C(T109A). Key residues involved in the structural rearrangement of the G interface are shown as ball-and-stick models. Yellow surface representation is used for GTP and GDP.
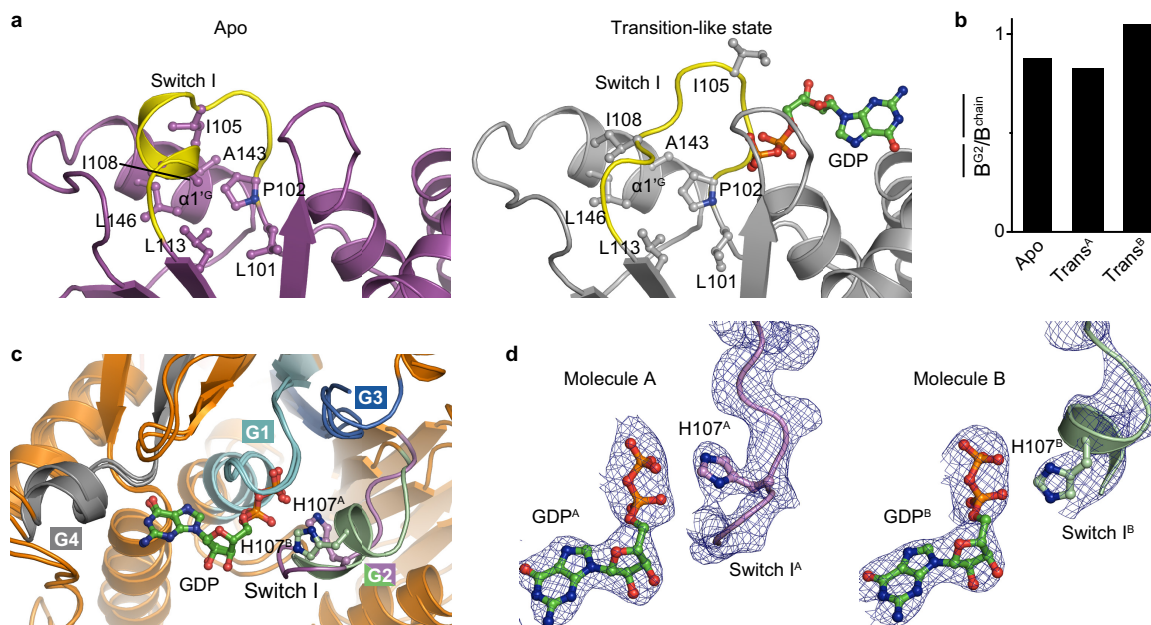
Extended Data Figure 7 | Analysis of the switch I conformations.
a, Configuration of switch I of $MFN1_{IM}$ in nucleotide-free and the transition-like states (molecule A of the dimer is used). Switch I is coloured yellow. Residues involved in the hydrophobic networks are shown as ball-and-stick models. Note the rearrangements of this region between the two states. **b**, Stability of switch I region of $MFN1_{IM}$ at different states. The stability of switch I is reflected by the mean B factor of the main-chain atoms of switch I compared to that of the whole peptide chain. $Trans^A$ and $Trans^B$ denote molecules A and B of the $MFN1_{IM}C$ dimer in the transition-like state, respectively. The switch I regions in both nucleotide-free and transition-like ($Trans^A$) states have relatively stable conformations with regard to the whole molecule. **c**, Superposition of the GTPase catalysis centres of two molecules of the $MFN1_{IM}C$ dimer in the transition-like state. The G1–G4 elements are as in Fig. 2b, except that the G2 element of the molecule B in pale green. His107 and is shown as ball-and-stick models. **d**, The electron density of the switch I regions in the two molecules of the $MFN1_{IM}C$ dimer. The density is shown as blue mesh at a contour level of 1.2σ for both molecules A (left) and B (right). His107 is shown as ball-and-stick models.
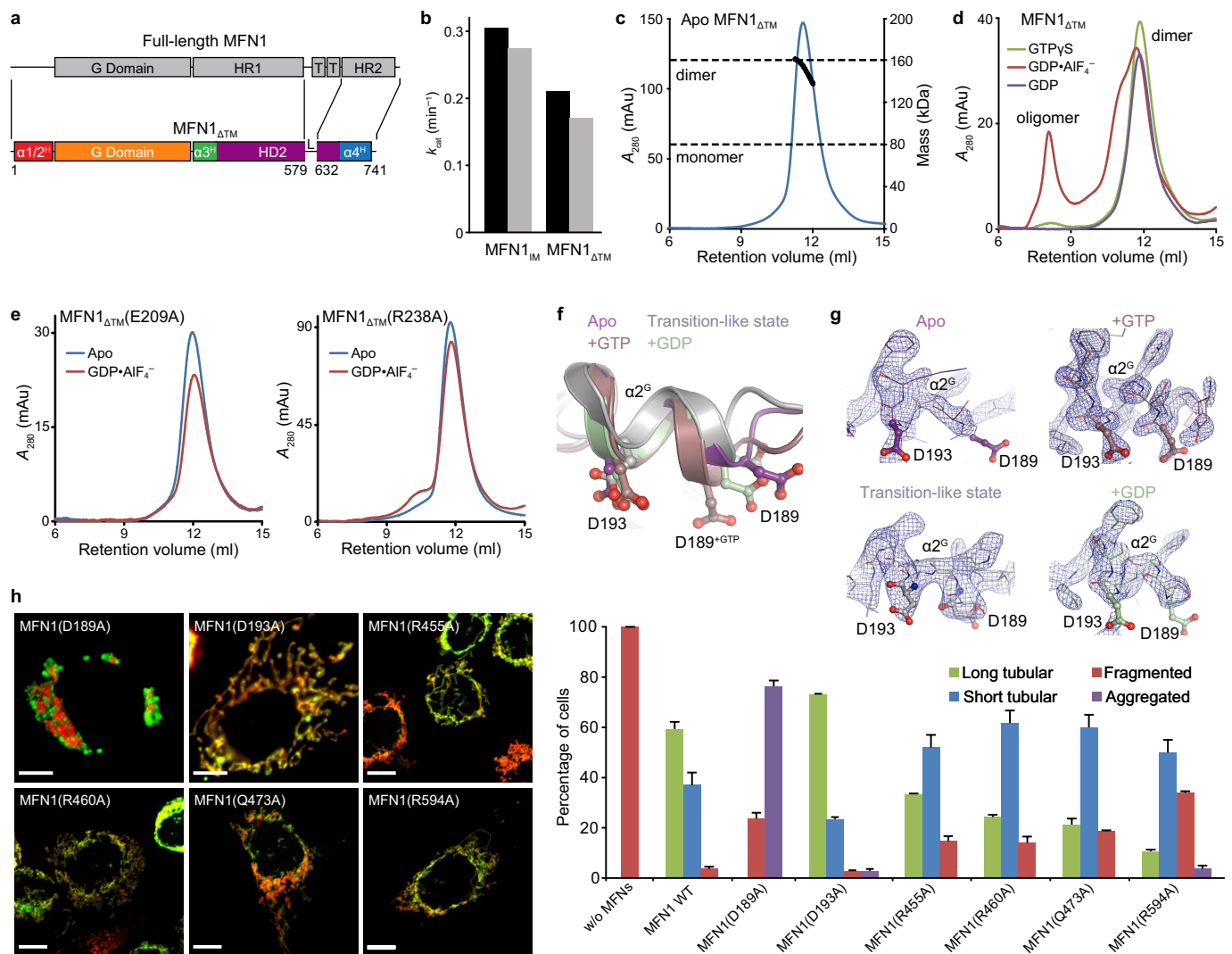
Extended Data Figure 8 | Characterization of MFN1$_{\Delta TM}$ and the Asp189 trigger. a, Schematic representation showing the strategy of generating the MFN1$_{\Delta TM}$ construct. Colour as in Fig. 1a, and HD2 is in purple. **b**, Comparison of GTPase activity between MFN1$_{IM}$C and MFN1$_{\Delta TM}$. Results from two separated experiments are presented for each protein. **c**, RALS analysis of MFN1$_{\Delta TM}$ showing that it is a stable dimer in nucleotide-free state. **d**, Analytical gel filtration results of MFN1$_{\Delta TM}$ in the GTPγS, GDP•AlF$_4^-$ and GDP-bound states. **e**, Analytical gel filtration results of MFN1$_{\Delta TM}$(E209A) and MFN1$_{\Delta TM}$(R238A) in nucleotide-free and GDP•AlF$_4^-$-bound states. Note that in the GDP•AlF$_4^-$-bound state, no peak at the exclusion volume is observed, indicating that both mutants do not oligomerize. **f**, Structural comparison of MFN1$_{IM}$ in different nucleotide-loading states at $\alpha 2^G$. Note the distinct orientation of Asp189 in the GTP-bound state, and the uniformly oriented Asp193. Asp193 is a conserved residue that also faces the predicted HD2. Colour as in Fig. 4g. **g**, Electron density of Asp189 and Asp193 on $\alpha 2^G$ in MFN1$_{IM}$

structures contoured at 1.0σ. Note the difference in orientations of $\alpha 2^G$ in these structures as revealed by the density maps. Although the side chain of Asp189 is not fully traceable in some non-GTP-bound cases, their locations would differ from that in the GTP-bound form. **h**, Mitochondrial elongation assay for the mutants in the plausible G-domain–HD2 contact. For each construct, 100 cells were scored in biological triplicate; representative images are shown. Error bars indicate s.e.m. Scale bars, 10 μm. Note that the clumping mitochondria for MFN1(D189A) and anticipated normal mitochondria for MFN1(D193A). Arg455, Arg460, Gln473 and Arg594 are conserved residues in the predicted HD2 which were screened for contacting Asp189 based on sequence alignment of mitofusins and BDLP. Corresponding mutants increased mitochondrial fragmentation or aggregation. It seems that either they are not the right residues interacting with D189, or a single point mutation was not sufficient to break the plausible interaction.

Extended Data Figure 9 | Proposed model for MFN1-mediated OMM fusion. a, Model for nucleotide-regulated OMM fusion mediated by MFN1. The G domain, HD1, predicted HD2 and transmembrane domain are indicated in the top left MFN1 molecule, and coloured orange, green, grey and blue, respectively. During GTP hydrolysis, HD2s of tethered MFN1 molecules may fold back via intrinsic mechanistic potential analogous to the BSE-stalk of MxA protein (Y.C. *et al.*, unpublished observations) to bring opposing membrane in close proximity. Repeating tethering reactions by appropriate numbers of MFN1 would promote docking of opposing OMMs, presumably as described in a recent *in vitro* electron cryo-tomography study where discrete electron densities representing yeast FZO1 displayed a ring-like arrangement surrounding docked OMMs[47]. If this 'docking ring' exists in mammals, MFN1 may

contribute to its formation through hydrolysis-dependent in *trans* oligomerization (shown in **c**). Subsequent membrane merger may rely on local membrane curvature, as reported in many cellular events such as synaptic vesicle fusion and cell-to-cell fusion[48,49]. As the space between docked OMMs (approximately 2 nm) is too small to accommodate MFN1 molecules[47], these molecules may gather at the rim of the docking site, resulting in a crowding effect that possibly generates bending on local OMMs to facilitate fusion[50,51]. **b**, Schematic drawing shows the GTP-loading-induced conformational rearrangement of the MFN1 HD1–HD2 region via the Asp189 trigger. **c**, Possible organization of the plausible in *trans* cross oligomer of MFN1 around the docking site. This process is dependent on GTP hydrolysis.

Extended Data Table 1 | Crystallographic data collection and refinement statistics

	MFN1$_{IM}$B	MFN1$_{IM}$B	MFN1$_{IM}$C^{T109A}	MFN1$_{IM}$C	MFN1$_{IM}$C^{T109A}	MFN1$_{IM}$A	MFN1$_{IM}$A
Initial ligand	GMPPCP	GMPPCP	GTP	GDP·AlF$_4^-$	GTP	GTPγS	GDP
State	apo	apo	GTP-bound	Transition-like	GDP-bound	GTPγS-bound	GDP-bound
Data collection							
Data Set	Native	SeMet derivative	Native	Native	Native	Native	Native
Space group	P2$_1$2$_1$2$_1$	P2$_1$2$_1$2$_1$	P2$_1$2$_1$2$_1$	C2	P2$_1$2$_1$2$_1$	C222$_1$	P3$_1$21
Cell dimensions							
a, b, c (Å)	51.8, 110.9, 112.4	51.6, 110.2, 111.3	70.6, 72.4, 95.3	104.1, 46.0, 146.2	70.4, 72.9, 95.0	127.6, 143.1, 159.0	93.6, 93.6, 114.1
α, β, γ (°)	90	90	90	92.2	90	90	120
Wavelength (Å)	0.91800	0.97915	0.97915	0.91800	0.97915	0.91800	0.91800
Resolution (Å)	47.0-2.2 (6.55-2.2)	49.7-2.3 (6.84-2.3)	44.7-1.6 (4.79-1.6)	48.7-2.8 (8.30-2.8)	44.7-1.8 (5.37-1.8)	47.7-6.1 (16.77-6.1)	46.8-4.3 (12.49-4.3)
R_{sym}*	0.068 (0.438)	0.060 (0.494)	0.043 (0.583)	0.066 (0.629)	0.048 (0.517)	0.0470 (0.522)	0.064 (0.537)
$I / σ(I)$	18.08 (4.27)	21.22 (4.14)	25.54 (3.33)	20.55 (3.02)	25.08 (4.12)	19.28 (3.32)	17.81 (4.62)
Completeness (%)	99.4 (98.1)	99.5 (97.7)	89.4 (99.7)	99.1 (97.0)	98.9 (98.8)	98.3 (99.8)	97.2 (95.0)
Redundancy	7.9 (8.0)	7.7 (7.5)	7.1 (7.2)	7.4 (7.4)	7.9 (8.1)	5.4 (5.4)	10.4 (10.8)
Refinement							
Resolution (Å)	39.5-2.2		29.1-1.6	48.7-2.8	29.0-1.8		
No. reflections	33374		57847	24264	45448		
R_{work} / R_{free}	0.175/0.214		0.179/0.215	0.201/0.258	0.177/0.204		
No. atoms							
Protein	3291		3224	6484	3137		
Ligand/ion	0		34	64	28		
Water	184		427	4	273		
B-factors							
Protein	57.5		33.6	106.9	43.4		
Ligand/ion	0		30.8	84.0	36.3		
Water	55.3		43.2	68.9	48.3		
R.m.s. deviations							
Bond lengths (Å)	0.007		0.005	0.012	0.006		
Bond angles (°)	0.753		0.812	1.471	0.763		

*Numbers in parentheses represent values from the highest resolution shell.